Distorted-Wave Born-Approximation Analysis of the $(d,{}^3\mathrm{He})$ Reaction on "Closed Shell" Nuclei*

J. C. HIEBERT†
Texas A and M University, College Station, Texas

AND

E. NEWMAN AND R. H. BASSEL‡
Oak Ridge National Laboratory, Oak Ridge, Tennessee

(Received 21 September 1966)

Angular distributions for $^{16}\mathrm{O}(d,{}^3\mathrm{He})^{15}\mathrm{N}$ and $^{40}\mathrm{Ca}(d,{}^3\mathrm{He})^{39}\mathrm{K}$ reactions were measured at an energy of 34.4 MeV. The applicability of the distorted-wave theory to these reactions and the ability to extract reliable spectroscopic factors was investigated. Calculations using the local zero-range, nonlocal, and finite-range formulations are compared with the data. The roles of $\mathbf{L}\cdot\mathbf{S}$ coupling, deuteron optical-model parameters, and radial cutoffs on the predicted shape and magnitude are presented. The local zero-range and finite-range forms of the theory give comparable spectroscopic factors, while the nonlocal calculations are consistently low. Deviations from the closed-shell description of the ground states of $^{16}\mathrm{O}$ and $^{40}\mathrm{Ca}$ are observed. Substantially all the $1p$ hole strength in $^{16}\mathrm{O}$ is found, and in $^{40}\mathrm{Ca}$ some deeper $l=2$ hole strength is seen. Results of $^{40}\mathrm{Ca}(d,t)^{39}\mathrm{Ca}$ reactions are also presented.

I. INTRODUCTION

DIRECT-REACTION studies have become a powerful tool for obtaining nuclear-structure information. In particular, deuteron-stripping reactions analyzed by means of the distorted-wave (DW) Born approximation[1,2] have been demonstrated to afford a reasonably precise measurement of spectroscopic information[3] concerning the single-particle neutron states of nuclei. Similar information has been obtained with the (p,d) and (d,t) pickup reactions. Only recently have corresponding direct reaction studies been undertaken to measure spectroscopic quantities describing single-particle or single-hole proton states of nuclei.[4–10] The (d,n) and (n,d) reactions allow the "simplest" theoretical interpretation but the technical difficulties involved in either producing monoenergetic neutron beams or detecting neutrons with high-resolution limit the usefulness of these reactions. Recent developments of high-resolution semiconductor detectors and intermediate energy accelerators have resulted in the use of $(d,{}^3\mathrm{He})$ and $({}^3\mathrm{He},d)$ reactions to study proton states.

Most $(d,{}^3\mathrm{He})$ reaction studies[6,10] to date have been initiated with low-energy deuteron beams. There are distinct advantages to be gained with higher incident energies. For a given l value, where l is the orbital angular momentum of the captured proton, the structure of the angular distribution becomes more pronounced and the peak-to-peak separation decreases with increasing energy. These two effects make it considerably easier to assign l values. In addition, the increased energy allows the study of states in heavy nuclei and tightly bound proton states where Coulomb barrier suppression and Q-dependent effects play important roles. In this investigation proton states bound by energies up to 18.5 MeV have been studied with apparent success in determining spectroscopic information. This paper reports an attempt to test the validity of applying the DW theory in the analysis of $(d,{}^3\mathrm{He})$ reactions at 34.4 MeV.

The doubly-magic, closed-shell nuclei $^{16}\mathrm{O}$ and $^{40}\mathrm{Ca}$ have been chosen for this study. The $(d,{}^3\mathrm{He})$ reactions proceeding to the ground states of the final-state nuclei $^{15}\mathrm{N}$ and $^{39}\mathrm{K}$ are believed to correspond to the removal of a proton from a closed $1p_{1/2}$ and $1d_{3/2}$ subshell, respectively. Thus, the spectroscopic factors $S(l,j)$ are predicted to be $S(1,\frac{1}{2})=2.0$ for $^{16}\mathrm{O}$ and $S(2,\frac{3}{2})=4.0$ for $^{40}\mathrm{Ca}$. Recent evidence indicates[11–14] that there are particle-hole excitations present in the ground-state wave functions of both $^{16}\mathrm{O}$ and $^{40}\mathrm{Ca}$. Nevertheless, these departures from the shell closures are small and the re-

* Research sponsored in part by the U. S. Atomic Energy Commission under contract with the Union Carbide Corporation.

† USAEC Postdoctoral Fellow under appointment from Oak Ridge Associated Universities, 1963–1965. Visting scientist at Oak Ridge National Laboratory, 1965–1966.

‡ Present address: Brookhaven National Laboratory, Upton, Long Island, New York.

[1] R. H. Bassel, R. M. Drisko, and G. R. Satchler, Oak Ridge National Laboratory Report No. ORNL-3240 (unpublished).

[2] G. R. Satchler, Nucl. Phys. **55**, 1 (1964).

[3] L. L. Lee, Jr., J. P. Schiffer, B. Zeidman, G. R. Satchler, R. M. Drisko, and R. H. Bassel, Phys. Rev. **136**, B971 (1964).

[4] B. Cujec, Phys. Rev. **128**, 2303 (1962).

[5] K. Ilakovac, L. G. Kuo, M. Petravic, I. Slaus, P. Thomas, and G. R. Satchler, Phys. Rev. **128**, 2739 (1962).

[6] J. L. Yntema and G. R. Satchler, Phys. Rev. **134**, B976 (1964).

[7] D. D. Arsmtrong and A. G. Blair, Phys. Letters **10**, 204 (1964); R. B. Day, A. G. Blair, and D. D. Armstrong, *ibid.* **9**, 327 (1964); A. G. Blair, Phys. Rev. **140**, B648 (1965); D. D. Armstrong and A. G. Blair, *ibid.* **140**, B1226 (1965).

[8] W. N. Wang and E. J. Winhold, Phys. Rev. **140**, B882 (1965).

[9] J. C. Hiebert, E. Newman, and R. H. Bassel, Phys. Letters **15**, 160 (1965).

[10] D. C. Shreve, C. D. Kavaloski, J. S. Lilley, and N. Stein, Bull. Am. Phys. Soc. **11**, 118 (1966).

[11] C. Glashausser, M. Kondo, M. E. Rickey, and E. Rost, Phys. Letters **14**, 113 (1965).

[12] R. Bock, H. H. Duhm, and R. Stock, Phys. Letters **18**, 61 (1965).

[13] D. Cline, W. P. Alford, and L. M. Blau, Nucl. Phys. **73**, 33 (1965).

[14] J. C. Hiebert, E. Newman, and R. H. Bassel, Bull. Am. Phys. Soc. **11**, 44 (1966).

quirement that the DW theory give correct absolute cross sections when including the above spectroscopic factors is still felt to be a very rigorous test of the theory. In addition, the test of the DW theory is made both for a light nucleus ^{16}O, where difficulties are often encountered in applying optical-model analyses, and for a medium-weight nucleus ^{40}Ca, where these problems are less important.

The present work attempts to study reaction systematics for the two ground-state transitions discussed above and for transitions to other single-hole states that are identified in ^{15}N and ^{39}K. For this purpose, spin-orbit coupling, nonlocal and finite-range interactions, and the problem of cutoffs in the radial overlap calculation are investigated in as much detail as presently available computer codes allow. After demonstrating the reliability of the DW theory for extracting spectroscopic information from $(d,{}^3\mathrm{He})$ data,[15] we are then able to present additional information concerning deviations from the doubly closed-shell description of these two nuclei.

The optical-model parameters used in the DW calculations were extracted from an analysis of deuteron elastic scattering from ^{16}O and ^{40}Ca at the same energy as the reaction studies. These analyses, as well as those for other targets, are to be published in a subsequent paper.[16] Unfortunately, the required elastic scattering of ^{3}He from ^{15}N and ^{39}K has not been measured. Since little is known about the systematics of optical potential parameters for ^{3}He scattering, extrapolations had to be made from the analyses presently available.[17]

It was possible to measure $^{40}\mathrm{Ca}(d,t)^{39}\mathrm{K}$ reaction yields at the same time $(d,{}^3\mathrm{He})$ data were being acquired. A brief comparison of these results with the $(d,{}^3\mathrm{He})$ study is also presented.

II. THEORY

We present here a brief review of the DW theory of the direct nuclear reaction $A(d,{}^3\mathrm{He})B$ to elicit the approximations inherent in the theory, and also those required by the present application of the theory in interpreting experimental data. The DW approximation to the exact transition amplitude[1] for a direct reaction takes the form

$$T=J\int d\mathbf{r}_d\int d\mathbf{r}_\tau \chi_\tau^{(-)*}(\mathbf{k}_\tau,\mathbf{r}_\tau) \times\langle B,d|\,V\,|A,{}^3\mathrm{He}\rangle\chi_d^{(+)}(\mathbf{k}_d,\mathbf{r}_d)\,, \quad (1)$$

where $\mathbf{r}_d$ is the separation of the centers of mass of A and d; similarly $\mathbf{r}_\tau$ for B and ^{3}He. The $\chi(\mathbf{k},\mathbf{r})$ are distorted waves describing the elastic scattering in the two channels, and J is the Jacobian of the transformation to the relative coordinates $\mathbf{r}_d$, $\mathbf{r}_\tau$. It should be remembered that the DW approximation, Eq. (1), proceeds from the observation that elastic scattering is the dominant process when two nuclei collide.

The nuclear matrix element $\langle B,d|\,V\,|A,{}^3\mathrm{He}\rangle$ is taken between the internal states of the colliding pairs and implies integration over all internal coordinates exclusive of $\mathbf{r}_d$ and $\mathbf{r}_\tau$. We use here the prior-interaction form of the potential,

$$V=V_{dA}-U_{dA}\,,$$

where U_{dA} is the optical potential chosen to describe the elastic scattering in the $d+A$ system, and thus cannot excite or rearrange this system. Since the nucleus A includes the proton to be picked up, leaving the residual nucleus B, V_{dA} can be separated so that

$$V=V_{dp}+V_{dB}-U_{dA}\,. \quad (2)$$

It is customary to take the interaction V_{dp} to be the important term for the $(d,{}^3\mathrm{He})$ reaction. It has been pointed out[3,6] in the discussion of stripping reactions that this approximation seems physically reasonable when one considers the inverse pickup reaction. However, the cancellation between the remaining terms in (2) cannot be complete. Since extended discussions of this problem have been presented elsewhere[1,3,18] and our intention is to test the validity of the DW theory using $V=V_{dp}$ in Eq. (1), we only re-emphasize the nature of this approximation. The main point is that V_{dB} can be considered a true, and therefore real, interaction whereas U_{dA} is an optical potential with an important imaginary term. Thus, U_{dA} can only produce elastic scattering while V_{dB} can also excite the core B. Even if V_{dB} were represented by an optical potential U_{dB}, the cancellation would not be entirely complete since the potentials refer to slightly different nuclei. Another related complication which is traditionally ignored is the presence of "exchange terms" which would arise in an antisymmetrized formulation of the transition amplitude (1).

Because most previous applications of the DW theory have been for stripping rather than for pickup reactions, it is convenient to relate the transition amplitude for the reaction $A(d,{}^3\mathrm{He})B$ to the inverse reaction $B({}^3\mathrm{He},d)A$ with reversed momenta and spins, but with the same quantization axes. This transformation has been formulated[1] and results in the differential cross section for the $(d,{}^3\mathrm{He})$ reaction,

$$\frac{d\sigma_{lj}}{d\Omega}(\theta)=\tfrac{2}{3}na^2(s)\left[\frac{D_0^2(d,p)}{1.018\times10^4}\right]C^2S(l,j)\sigma_{lj}(\theta)\,. \quad (3)$$

[15] Although the present discussion is restricted to the $(d,{}^3\mathrm{He})$ reaction, the conclusions as to the usefulness of the DW theory apply equally well to $({}^3\mathrm{He},d)$ stripping reactions.

[16] E. Newman, L. C. Becker, B. M. Preedom, and J. C. Hiebert, (to be published).

[17] W. E. Burcham, D. J. Baugh, P. M. Rolph, and S. M. Scarrott, Bull. Am. Phys. Soc. **10**, 1203 (1965).

[18] K. R. Greider, in *Proceedings of the Third Conference on Reactions Between Complex Nuclei, Asilomar, 1963,* edited by A. Ghiorso, R. M. Diamond, and H. E. Conzett (University of California Press, Berkeley, California, 1963), p. 148.

The quantity $na^2(s)D_0^2(d,p)$ refers to the overlap of the $d+p$ and ^{3}He systems; C is the isotopic spin Clebsch-Gordan coefficient

$$C=\langle T_B\tfrac{1}{2},\ M-mm|\,T_A,M\rangle,$$

where $M=T_A=\frac{1}{2}(N-Z)$ of the target, $m=-\frac{1}{2}$, and $S(l,j)$ is the usual spectroscopic factor. For the two $Z=N$ nuclei to be considered below, $C^2=\frac{1}{2}$, and $C^2S(l,j)$ is the number of protons present in the (l,j) shell of the target nucleus. The normalization of Eq. (3) is chosen to agree with the DW computer programs TSALLY[1] and JULIE[19] which calculate $\sigma_{lj}(\theta)$. The quantity $D_0^2\times(1.018\times10^4)^{-1}$ is unity for the case of (d,p) reactions calculated in the zero-range approximation. The quantity $na^2(s)$ in Eq. (3) is the product of the number of equivalent nucleons and the square of the coefficient of fractional parentage for decomposing the ^{3}He particle into a deuteron plus an odd proton. In the approximation that the ^{3}He ground state is a pure $(1s)^3$ nucleon configuration and the deuteron ground state is a pure $^3S_1$ state, $na^2(s)=\frac{3}{2}$. The remaining term in the expression for the differential cross section (3) is the radial overlap integral

$$D(r)=\int d\rho\ \psi_d^*(\rho)V_{dp}\psi_{^3\mathrm{He}}(r,\rho)=D_0F(r),\qquad(4)$$

where $F(r)$ is the range function.[1] This integral has recently been evaluated by Bassel[20] in both the zero-range and finite-range approximations. In these calculations the classic Hulthén wave function for the deuteron and the Irving-Gunn[21] wave function for the ^{3}He system have been used, resulting in

$$D_0^2(\text{zero-range})=2.59\times10^4\ \text{MeV F}^3,\qquad(5a)$$

$$D_0^2(\text{finite-range})=2.99\times10^4\ \text{MeV F}^3.\qquad(5b)$$

Including all numerical factors, Eq. (3) for the $(d,^3\mathrm{He})$ differential cross section becomes

$$\frac{d\sigma_{lj}}{d\Omega}(\theta)=2.95C^2S(l,j)\sigma_{lj}(\theta).\qquad(6)$$

D_0^2 (finite-range) has been used in Eq. (6) since it corresponds to a more correct calculation of the overlap integral (4). Thus, Eq. (6) will be used as the normalized differential cross section irrespective of the approximation used in calculating $\sigma_{lj}(\theta)$.

The "reduced" cross section $\sigma_{lj}(\theta)$, as calculated by the DW theory, is proportional to the sum of the squares of the amplitudes $\beta_j{}^{lm}$,

$$\sigma_{lj}(\theta)\propto\textstyle\sum_m|\beta_j{}^{lm}|^2,$$

where

$$\beta_j{}^{lm}=\frac{i^{-l}k_\beta{}^2}{[4\pi(2l+1)]^{1/2}}\left(\frac{M_A}{M_B}\right)^2\int\int\chi_\beta{}^{(-)*}(\mathbf{k}_\beta,\mathbf{r}_\beta)f_{ljm}(\mathbf{r}_\beta,\mathbf{r}_\alpha)\times\chi_\alpha{}^{(+)}(\mathbf{k}_\alpha,\mathbf{r}_\alpha)d\mathbf{r}_\alpha d\mathbf{r}_\beta.\qquad(7)$$

The form factor, f_{ljm}, is closely related to the wave function of the picked-up proton. In the zero-range approximation

$$f_{ljm}(\mathbf{r}_\beta,\mathbf{r}_\alpha)\simeq F_{lj}(r_\alpha)Y_l{}^{m*}(r_\alpha)\delta\left(r_\beta-\frac{M_A}{M_B}r_\alpha\right),\qquad(8)$$

and $F_{lj}(r)$ is the radial wave function of the picked-up proton.

Thus, to evaluate the reduced cross section three quantities must be determined: the wave functions in the entrance and exit channels, and the proton bound-state wave function. It is now possible to calculate each of these three quantities with or without spin-orbit coupling,[1,3,19] and with nonlocal potentials.[22] We can also treat the effective interaction either in zero-range or finite-range[23] approximation. It is the goal of the present work to test the predictions of the DW theory in these approximations against experiment to determine which form of the theory is most reliable for extracting spectroscopic information.

A. Spin-Orbit Effects

Spin-orbit coupling affects the $(d,^3\mathrm{He})$ differential cross section through each of the three quantities contained in the overlap integral (7). Spin-orbit distortions occur in the incident channel, the bound state function, and the exit channel. The most important consequence of these distortions is a change in the magnitudes of the cross sections. A weaker effect is the j dependence of the shape of angular distributions which is manifest at large angles. This latter effect has been studied mostly with (d,p) reactions,[3,11,24] and can be reproduced qualitatively by including spin-orbit distortions in the DW theory.

The effects on the magnitude of the cross section due to spin-orbit coupling are better understood. Inclusion of a spin-orbit term in the shell-model potential that binds the proton to be picked up from the target nucleus results in different wave functions for $j=l\pm\frac{1}{2}$. When $j=l+\frac{1}{2}$, the spin-orbit potential is attractive and the tail of the bound-state function extends out further and enhances the cross section. For $j=l-\frac{1}{2}$, the inverse occurs. In the ^{40}Ca(d,p) study[3] the effect on the cross section is about $\pm25\%$ for $l=3$ and $\pm5\%$ for $l=1$. It is expected that the effect will be larger for $(d,^3\mathrm{He})$ reac-

[19] R. M. Drisko, R. H. Bassel, and G. R. Satchler (unpublished).
[20] R. H. Bassel, Phys. Rev. **149**, 791 (1966).
[21] J. C. Gunn and J. Irving, Phil. Mag. **42**, 1353 (1951).
[22] F. G. Perey and D. S. Saxon, Phys. Letters **10**, 107 (1964); F. G. Perey and B. Buck, Nucl. Phys. **32**, 353 (1963).
[23] R. M. Drisko and G. R. Satchler, Phys. Letters **9**, 342 (1964).
[24] L. L. Lee, Jr. and J. P. Schiffer, Phys. Rev. Letters **12**, 108 (1964); Phys. Rev. **136**, B405 (1964).

tions because of the Coulomb barrier and also larger for more tightly bound particles. This effect has been investigated with the ^{40}Ca(d,^{3}He) reaction at 21.5 MeV.[6] It was found that neglecting spin-orbit effects on the proton bound state in zero-range DW calculations results in a change of cross section of about $\pm 20\%$ for $j=l\pm\frac{1}{2}$ with $l=2$.

A smaller effect is observed in the same ^{40}Ca(d,p) reaction mentioned above because of spin-orbit coupling in the distorted waves. In that study, the effect of including spin-orbit coupling in the scattering was considered separately for the entrance and exit channels, In either case, the effect was a 5–7% difference in the predicted peak cross section for $l=3$ stripping. The effect of spin-orbit coupling in ^{3}He scattering is still not well understood. Present information indicates that no spin-orbit coupling is required to fit elastic-scattering data.[25]

B. Zero-Range Approximation

Most DW calculations in the past have been made using the zero-range approximation, whereby the radial overlap integral (4) is replaced by

$$D(\mathbf{r}_{pd}) \approx D_0 \delta(\mathbf{r}_{pd}), \tag{9}$$

and the bound-state-function form factor of Eq. (8) is used. Since the more complete calculations including finite-range and nonlocality effects are now available, our purpose is to compare the predictions of the zero-range approximation with experiment, and with the predictions of the more complete calculations. These comparisons may enable groups who have computer codes based on the zero-range theory to make appropriate corrections to these predictions. Again, we emphasize the point that in all zero-range calculations reported below, the value of D_0 obtained in the finite-range calculation (5b) is used in Eq. (9).

C. Nonlocal Calculations

It has been demonstrated that there is good reason for believing that the optical-model and shell-model potential wells are nonlocal.[22,26] Perey and Buck[22] have demonstrated that the scattering from a nonlocal optical potential can be reproduced by an equivalent local potential whose parameters vary with the bombarding energy. An additional result, termed "the Perey effect,"[22,27] is that the eigenfunctions of the nonlocal potential are reduced in the nuclear interior in comparison to the eigenfunctions of the equivalent local potential. This reduction can be reproduced, to a good approximation, with a damping factor obtained from the local energy approximation (LEA),[27,28]

$$N(r)=C[1-(\mu\beta^2/2\hbar^2)U(r)]^{-1/2}, \tag{10}$$

where μ is the reduced mass of the particle, β the nonlocality range, $U(r)$ is the equivalent local potential, and C is a normalizing constant equal to one for the scattered functions and greater than one for bound orbitals. Values for β deduced from the energy dependence of local optical potentials are $\beta\sim 0.85$ F for nucleons,[22] $\beta\sim 0.54$ F for deuterons, and $\beta\sim 0.2$ F for alpha particles.[27]

These corrections can be very important since the DW matrix element contains two distorted-wave correction factors and one from the nuclear form factor. Thus, there can be very important reductions in the contributions to the reaction from the nuclear interior. In reactions including strongly absorbed particles such as the (d,^{3}He) case under consideration, the net effect of nonlocality is to increase the reaction cross section because of the increased magnitude of the bound-state wavefunction tail.

D. Finite-Range Effects

An exact finite-range DW calculation[29] of stripping and pickup reactions requires a prohibitive amount of computation. Thus the introduction of the LEA to the finite-range effects[28,30] has been most welcome since this approximation yields a radial correction factor to be included in the usual zero-range calculation. This correction factor for the reaction $A(d,^3\mathrm{He})B$ takes the form

$$\Lambda(r)=1-\left[U_{^3\mathrm{He}}(r)-U_p(r)-U_d\left(\frac{rM_B}{M_A}\right)-S(^3\mathrm{He})\right]\Big/ 2(\hbar^2/MR^2)\cdot(M_{^3\mathrm{He}}/M_dM_p). \tag{11}$$

Here $U_i(r)$ is the optical potential for the particle i, M is an atomic mass unit, S is the separation energy of the proton from ^{3}He leaving the deuteron, and R is the "range" defined in Ref. 10. One sees from Eq. (11) that the finite-range correction is smallest if the potential operating on the ^{3}He particle is roughly the sum of the potentials operating on its constituents, $U_{^3\mathrm{He}}\sim U_d+U_p$. Another interesting feature is that the correction does not vanish at large distances due to the separation energy term. The accuracy of the LEA has been verified in some typical cases by comparison with exact calculations,[29] and has been checked for the reaction leading to the ^{39}K ground state.

The inclusion of finite-range corrections in direct

[25] D. D. Armstrong, A. G. Blair, and R. H. Bassel (to be published).
[26] N. Austern, Phys. Rev. **137**, B752 (1965).
[27] F. G. Perey, in *Proceedings of the Rutherford Jubilee International Conference, Manchester, England, 1961*, edited by J. B. Birks (Heywood and Company, Ltd., London, 1962), p. 125.
[28] P. J. A. Buttle and L. J. B. Goldfarb, Proc. Phys. Soc. (London) **83**, 701 (1964); G. Bencze and J. Zimanyi, Phys. Letters **9**, 246 (1964); F. G. Perey and D. Saxon, *ibid.* **10**, 107 (1964).
[29] N. Austern, R. M. Drisko, E. C. Halbert, and G. R. Satchler, Phys. Rev. **133**, B3 (1964).
[30] J. K. Dickens, R. M. Drisko, F. G. Perey, and G. R. Satchler, Phys. Letters **15**, 337 (1965).

reaction calculations produces results very similar to nonlocal effects as discussed above. This is apparent in the LEA since the same type of damping factors, Eqs. (10) and (11), produce the corrections.

E. Radial Cutoffs

In applying DW theory to experimental data, the problem of whether or not to use radial cutoffs arises. The arguments for using such cutoffs concern the physical significance of optical-model wave functions in the region of the nuclear interior for complex particles.[3,6,31] If it is assumed that a deuteron or ^{3}He is strongly distorted in crossing the nuclear surface, then it can be argued that the nuclear interior should be excluded from the stripping integrals through the use of a radial cutoff.

However, the nonlocal and finite-range versions of the DW theory have been shown to lead to considerable damping of the contributions from the nuclear interior. The use of a cutoff in these calculations is definitely incorrect.[30] Indications are that these corrections give a better description of stripping and pickup reactions than does the zero-range approximation.[30,31] The smooth damping factors which result from including finite-range and nonlocal effects are preferable to arbitrary, sharp cutoffs.

F. Bound-State Functions

A serious problem associated with both the shapes and magnitudes of the predicted cross sections is the choice of the proper bound orbital to be used in the calculations. If the target or residual nucelus has a closed shell structure this function is a "true" single-particle (hole) wave function. In this situation the orbital is an eigenfunction of the self-consistent Hartree-Fock potential, which, it is generally believed, can be reasonably represented by the Woods-Saxon shape.

If the nucleus involved is not ideal, its structure must be taken into account in computing the effective "single" particle form factor. The problem is exceedingly complicated. An orderly procedure has been discussed by Pinkston and Satchler,[32] but no general solution is possible; each case must be treated individually.

In the present study we consider two extreme approximations. In the first, the orbital is considered to be an eigenfunction of a Woods-Saxon well with the binding energy equal to the separation energy.[32–36] This prescription has the virtue of yielding an eigenfunction with the correct asymptotic shape, but, except for single-particle states, the nuclear interior is not properly treated.

A second prescription for the wave function is to consider it an eigenfunction of the self-consistent potential which generates the "true" single-particle wave function, i.e., the shell-model potential.[32–36] Such a recipe does not take into account configuration mixing and is correct only for closed shell or closed shell plus one nuclei. For all other nuclei it is in principle incorrect since, as stressed by Pinkston and Satchler, it does not yield the proper asymptotic shape. This prescription is tested below with 2-particle–2-hole configurations found in the ^{16}O and ^{40}Ca ground states. For example, the reaction proceeding to the second excited state of ^{39}K requires, in first order, the admixture of a $(2d_{3/2})^{-2}$-$(1f_{7/2})^2$ proton configuration in ^{40}Ca. The effective energy is obtained for this case by calculating the $1f_{7/2}$ orbital as an eigenfunction of the same well that binds a $2d_{3/2}$ proton in ^{40}Ca with the proper separation energy.

A further assumption in either of these treatments is that the average well that binds the nucleon is spherical. By the same token we assume that the reaction is dominated by the direct stripping mode, i.e., core excitation is a negligible effect for the cases studied here. Since strongly absorbed particles show enhanced excitation of collective states in inelastic scattering, a two-step process is certainly possible. However, recent studies indicate[31,35] that this contribution is small and unimportant if the final state has good single-particle character.

Finally, even if the Woods-Saxon shape is representative of the single-particle well, its parameters are not well determined. The single-particle wave function is dependent on the radius and diffusivity parameters and the spin-orbit depth as well as on the binding energy. All calculations below use for the radius ($1.2A^{1/3}$ F) and diffuseness (0.65 F), the values determined from the optical potential which describes proton scattering[3] from ^{42}Ca, and which also gives a good account[3] of the ^{40}Ca(d,p) and ^{48}Ca$(^3$He$,d)$ reactions.[7]

III. EXPERIMENTAL PROCEDURE

Differential cross sections were measured at laboratory angles between 10° and 45° for the ^{16}O$(d,^3$He$)^{15}$N and ^{40}Ca$(d,^3$He$)^{39}$Ca reactions to ground and excited states with the beam from the Oak Ridge Isochronous Cyclotron. The energy was 34.4 MeV for the ^{16}O reactions and 34.2 MeV for ^{40}Ca. The ^{16}O targets were either 0.25 mil Mylar or CaO_2 about 0.5 mg/cm^2 thick. Calcium targets were self-supporting foils and were also about 0.5 mg/cm^2 thick.[37] The beam energy was determined by measuring the lab angle at which deuterons elastically scattered from hydrogen have the same energy as those inelastically scattered from the 4.43-MeV

[31] G. R. Satchler (to be published).
[32] W. T. Pinkston and G. R. Satchler, Nucl. Phys. **72**, 641 (1966).
[33] N. Austern, Phys. Rev. **136**, B1743 (1964).
[34] R. Sherr, B. F. Bayman, E. Rost, M. E. Rickey, and C. G. Hoot, Phys. Rev. **139**, B1272 (1965).
[35] P. Iano and N. Austern, Bull. Am. Phys. Soc. **9**, 665 (1964); Phys. Rev. **151**, 853 (1966); S. K. Penny and G. R. Satchler (to be published).
[36] J. L. Yntema, Phys. Rev. **131**, 811 (1963).

[37] We are grateful to J. G. Couch for providing these targets.

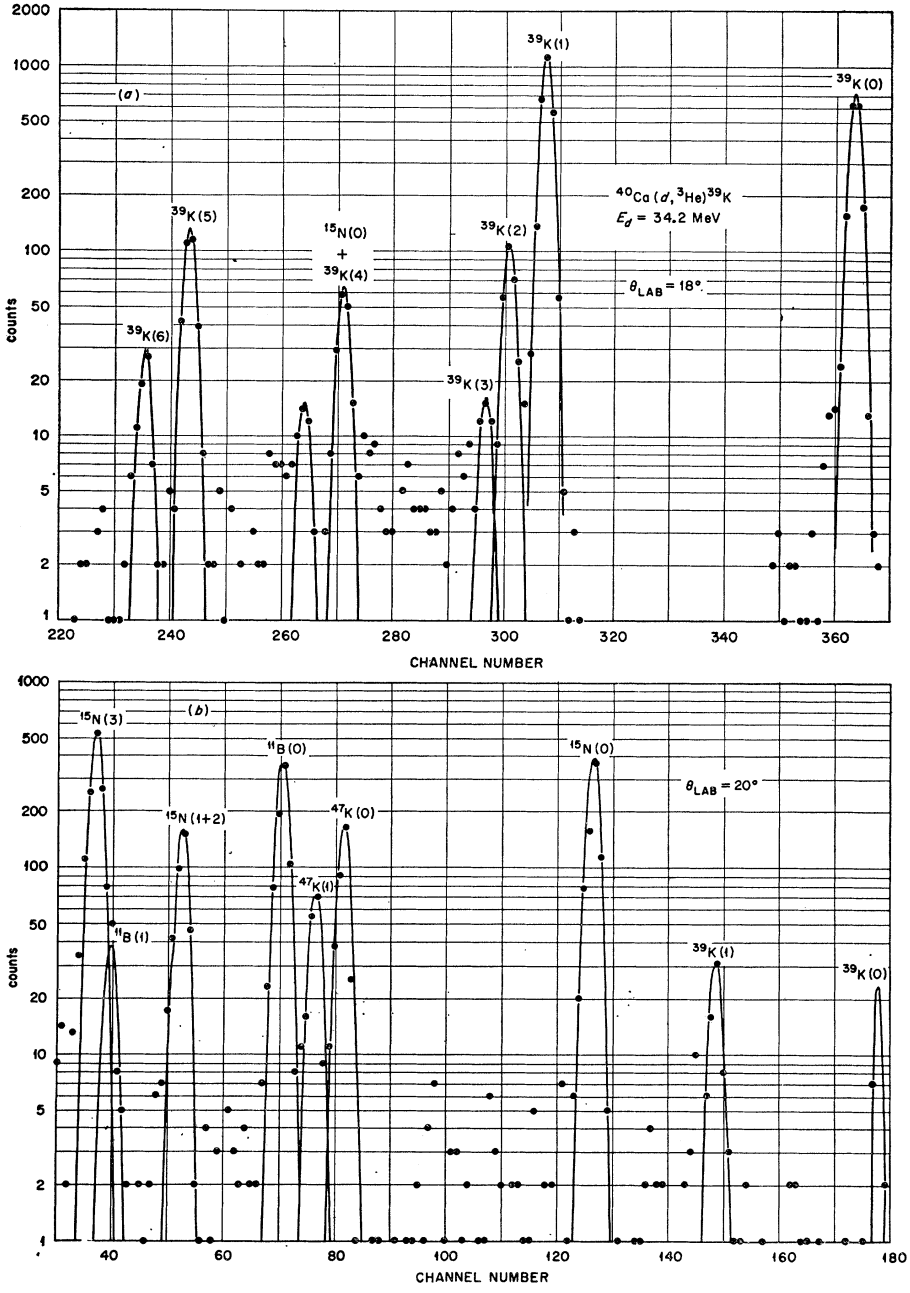

FIG. 1. Pulse-height spectrum of ^{3}He particles resulting from $(d,{}^3\mathrm{He})$ reactions in (a) a slightly oxidized ^{40}Ca target and (b) a ^{48}CaO target on a ^{12}C backing. Solid curves represent Gaussian distributions fit to the major reaction peaks. The final states are as indicated at each peak with the exception that ^{39}K(4)-^{39}K(6) refer to the 4th–6th observed states in ^{39}K rather than the 4th–6th excited states of ^{39}K.

state in ^{12}C. A polystyrene target was used for the energy measurements. The beam energy could be measured to ± 0.1 MeV with this technique.

The scattered reaction products were detected in a semiconductor ΔE-E detector telescope for particle identification. A 300-μ surface-barrier detector was used as the ΔE detector and a 500-μ surface barrier was used as the E detector. This combination of detectors allowed the observation of ^{3}He particles of $E=22$–38 MeV. For the ^{40}Ca(d,t) reactions that are briefly reported herein, a 1-mm surface-barrier detector was used as the stopping counter with $(d,{}^3\mathrm{He})$ and (d,t) data being accumulated simultaneously. The E and ΔE pulses were added at the amplifier input and ΔE versus $(E+\Delta E)$ spectra were recorded in a 20 000-channel, three-dimensional pulse-height analyzer. The observed ^{3}He energy resolution varied from 90 to 150 keV full width at half-maximum (FWHM) depending on target thickness, with the incident-beam spread contributing about 75 keV. Typical energy spectra are shown in Fig. 1. Relative errors are indicated in the experimental angular distributions. Where not shown as error bars, the errors fall

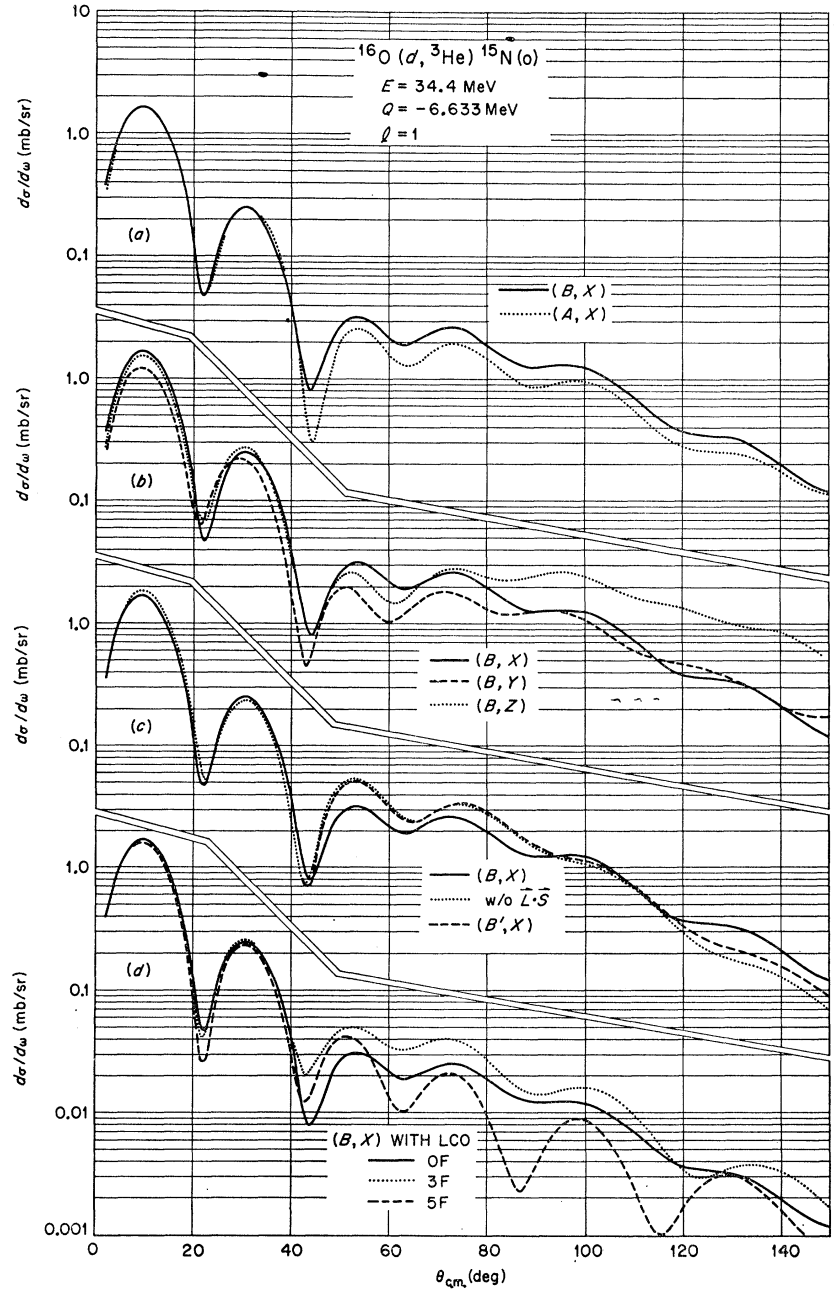

FIG. 2. Comparison of various DW predictions for the $^{16}O(d,{}^3He)^{15}N(0)$ reaction: (a) compares the best and average deuteron potentials, (b) shows the prediction using the three ^3He potentials of Table II, (c) shows the effects of spin-orbit coupling, and (d) shows the effects of including a lower cutoff in the radial integrations. The predictions are identified with a notation where (B,X) refers to the use of deuteron potential B in the incident channel and ^3He potential X in the exit channel.

within the data points. For both the ^{16}O and ^{40}Ca reactions, the cross sections have been normalized to the absolute deuteron elastic-scattering cross sections. It is estimated that the error in the absolute cross section is less than 20%.

IV. COMPARISON OF EXPERIMENT WITH THEORY

In any discussion concerned with the extraction of reliable spectroscopic information from a comparison of the DW theory and experiment, the following points must be considered. First, the shape of the predicted angular distributions should be compared with experiment to investigate the effect of the optical-model potentials used, spin-orbit coupling, the use of cutoffs, and the approximation used in calculating the radial overlap integrals. Following that, the effects of the above variations on the magnitude of the spectroscopic factors must be evaluated. Below, we compare the predictions of the DW theory with experimental data for the $(d,{}^3He)$ reactions proceeding to the ground state of ^{15}N, designated N(0), the third excited state of ^{15}N, N(3), and the ground state of ^{39}K, K(0).

TABLE I. Optical-model parameters for deuteron scattering at 34.4 MeV.[a]

Potential	Target	V_0 (MeV)	r_0 (F)	a (F)	$4W_d$ (MeV)	r_g (F)	b (F)	V_s (MeV)	$\chi^{2\,b}$
B	^{16}O	91.1	1.053	0.787	33.6	1.361	0.767	7.0	10
B'	^{16}O	92.0	1.053	0.771	32.7	1.361	0.772	0	11
A	^{16}O	97.3	1.0	0.735	36.0	1.35	0.764	7.0	92
B	^{40}Ca	111	0.981	0.829	44.6	1.363	0.769	7.0	4
B'	^{40}Ca	111	0.981	0.822	57.9	1.363	0.681	0	9
A	^{40}Ca	108	1.0	0.797	45.2	1.32	0.792	7.0	31

[a] For all potentials $r_c=0.986$ F.
[b] The quantity χ^2 is a measure of the goodness-of-fit of theory to data. It is defined in Eq. (13).

A. Deuteron Optical Potentials

Deuteron elastic scattering has been studied in great detail over the past few years.[38] These studies have shown that there are several ambiguities in the choice of optical potentials. Probably the most troublesome is the series of potentials with different real well depths that give the same scattering and differ, roughly, in the number of half-wave lengths inside the nucleus.[39] In the ^{40}Ca(d,p) study,[3] it was found that, of the many ambiguous potentials, the potential with a real well depth of order 100 MeV gave the most consistent results for angular distributions and spectroscopic factors. This result is gratifying since one would hope that the deuteron potential approximates the sum of the neutron and proton optical potentials, appropriately averaged. A study of deuteron scattering at 34.4 MeV has been conducted to obtain a consistent set of optical model parameters for the DW analysis of $(d,{}^3\mathrm{He})$ reactions.[16] This study was restricted to the "100-MeV" potential, and a set of average optical model parameters as a function of Z and A for nuclei with $A<100$ was obtained.

The general form of the optical potential used is

$$U(r)=U_c(r)-V_0(1+e^x)^{-1}-W_0(1+e^{x'})^{-1}$$
$$+4iW_D\left(\frac{d}{dx'}\right)(1+e^{x'})^{-1}+\left(\frac{\hbar}{m_\pi c}\right)^2\left(\frac{V_s}{r}\right)$$
$$\times(\mathbf{L}\cdot\mathbf{S})\frac{d}{dx}(1+e^x)^{-1}, \quad (12)$$

where

$$x=(r-r_0A^{1/3})/a, \quad x'=(r-r_0A^{1/3})/b,$$

and U_c is the Coulomb potential between a point-charge light particle and a uniformly charged sphere of radius $R_c=r_cA^{1/3}$. As is customary for the analysis of deuteron scattering, we have adopted the surface-absorption form and thus set $W_0=0$ in Eq. (12). The best-fit parameters, labeled B, and a set of average parameters, labeled A,[16] for the ^{16}O(d,d) and ^{40}Ca(d,d) are listed in Table I. Comparisons of the DW predictions for the $(d,{}^3\mathrm{He})$ reactions for these two sets of potentials are shown in Fig. 2(a) for the N(0) state, Figs. 3(a) for the N(3) state, and Fig. 4(a) for the K(0) state. These predictions are

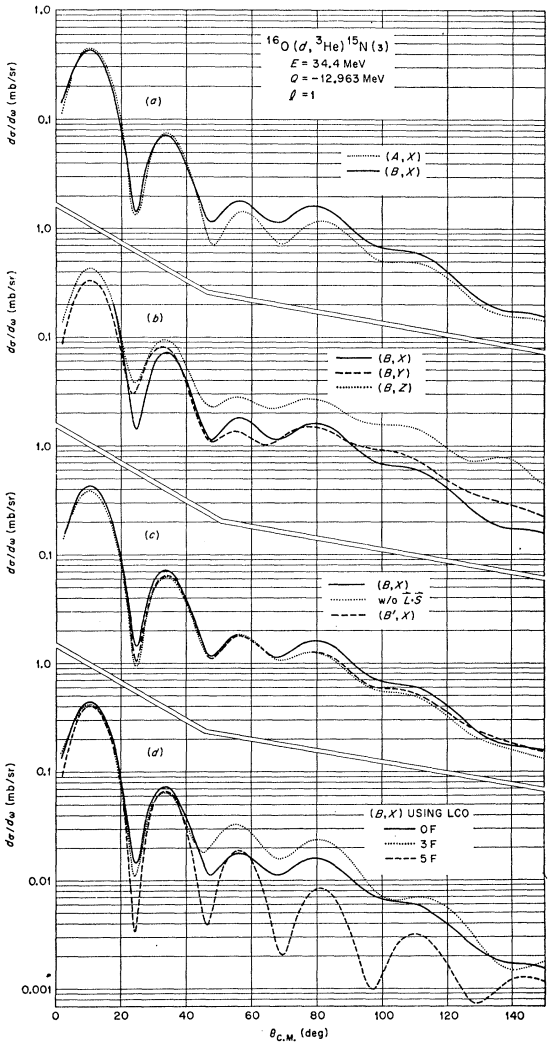

FIG. 3. Comparison of various DW predictions for the ^{16}O$(d,{}^3$He$)^{15}$N(3) reaction. See Fig. 2 caption.

[38] M. A. Melkanoff, T. Sarvada, and N. Cindro, Phys. Letters **2**, 98 (1962); C. M. Perey and F. G. Perey, Phys. Rev. **132**, 755 (1963); E. C. Halbert, Nucl. Phys. **50**, 353 (1964); J. K. Dickens and F. G. Perey, Phys. Rev. **138**, B1080 (1965); **138**, B1083 (1965).
[39] R. M. Drisko, G. R. Satchler, and R. H. Bassel, Phys. Letters **5**, 347 (1963).

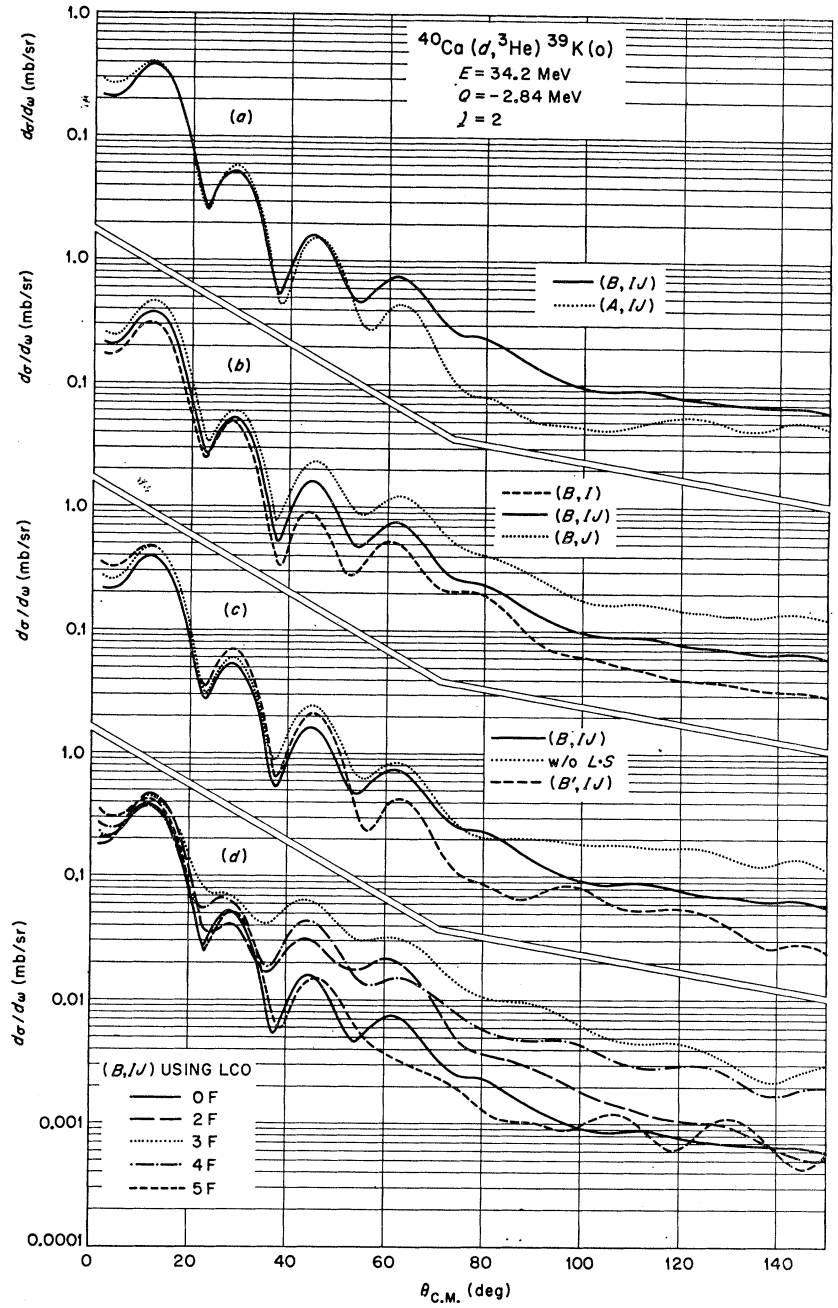

FIG. 4. Comparison of various DW predictions for the ^{40}Ca$(d,^3$He$)^{39}$K(0) reaction. See Fig. 2 caption.

based on the local zero-range approximation, without a lower cutoff, and use the best estimate of ^{3}He optical-model potentials. The choice of the ^{3}He parameters will be discussed in the next section.

The comparisons clearly show that the average parameters give a good description of the angular distributions and, indeed, essentially reproduce the shape and magnitude of the best-fit parameters for $\theta_{c.m.} \lesssim 40°$. For the N(0) reaction, a $1p_{1/2}$ proton pickup is assumed. The spectroscopic factor extracted using the average deuteron potential is only 1% smaller than the best fit potential result. Assuming a $1p_{3/2}$ proton pickup[40] for the N(3) reaction, the average potential spectroscopic factor is 2% less than the best fit result. For K(0), assuming a $1d_{3/2}$ pickup, the average result is 5% less than the best fit result. Thus, it is felt that the average deuteron potential can be used with some confidence for $(d,^3$He) predictions at 34.4 MeV in the absence of deuteron elastic-scattering measurements. Further comparisons are being made for $40<A<90$ to check the

[40] See the discussion in Sec. VB below.

TABLE II. Optical-model parameters for ^{3}He scattering.[a]

Potential	Target	Energy (MeV)	V_0 (MeV)	r_0 (F)	a (F)	W_0 (MeV)	r_0 (F)	b (F)
X	^{14}N	29	169	1.14	0.675	32.1	1.82	0.566
Y	^{16}O	10.5	170	1.03	0.893	20.0	2.06	0.510
Z	^{16}O	29	190	1.14	0.675	11.2	2.17	0.426
I	^{40}Ca	22	157	1.18	0.707	11.5	1.96	0.830
IJ[b]	^{40}Ca	30	167	1.16	0.715	13.0	1.80	0.872
J	^{40}Ca	37.7	177	1.14	0.723	14.5	1.64	0.910

[a] For all potentials $r_c=1.40$ F and $V_s=0$.
[b] Interpolated between the 22-MeV potential and the 37.7-MeV potential.

reliability of average-potential predictions in this region.[41]

B. ^{3}He Optical Potentials

A point of some concern in the test of the validity of the DW theory in analyzing $(d,{}^3\mathrm{He})$ reactions is the lack of knowledge of the ^{3}He optical potential. The ^{3}He energies involved in the present experiment range from 20 to 28 MeV for ^{15}N and 23 to 32 MeV for ^{39}K. Systematic studies of ^{3}He elastic scattering have only just been initiated.[42–44] Thus, for the ^{15}N+^{3}He system, three different potentials have been used. Potential X corresponds to 29-MeV ^{3}He scattering from ^{14}N; potential Y to 10.5-MeV ^{3}He scattering from ^{16}O; and potential Z to 29-MeV ^{3}He scattering from ^{16}O. These potentials are given in Table II. The traditional form of the optical potential, Eq. (12), for ^{3}He scattering with only volume absorption, i.e., $W_D=0$, is used. In Figs. 2(b) and 3(b) a comparison is made of the predictions using these three ^{3}He potentials for the ^{15}N ground-state and third-excited-state reactions, respectively. The best-fit deuteron potential is used in the incident channel in all cases.

The shape of the predicted angular distributions is quite similar in the region less than 50° for the N(0) reaction, Fig. 2(b). The magnitudes of the predictions vary considerably, particularly for the case of potential Y. This is not surprising since potential Y results from 10.5-MeV ^{3}He scattering, whereas the ^{3}He particles in the exit channel for the N(0) reaction have $E\approx 28$ MeV. For the N(3) reaction, there is considerable variation in shape among the three predictions, Fig. 3(b). For this transition the $1p_{3/2}$ proton is bound by 18.5 MeV and the outgoing ^{3}He particles have $E\approx 21$ MeV. Thus, none of the potentials under consideration would be expected to correspond to the actual exit channel scattering for this case. To demonstrate the shape-versus-energy dependency of the predicted angular distributions, we show a least-squares fit of the predictions to the experimental angular distribution in Fig. 5. Included, in addition to potentials X, Y, and Z, is an interpolated potential YZ. This crude interpolation assumes that the variation in the real- and imaginary-well parameters of potentials Y and Z is a linear function of the ^{3}He energy. Thus, as seen from Fig. 5, there is a factor of 4 variation in the degree to which the predictions reproduce the shape of the measured angular distributions, as indicated in the figure by χ^2, defined as

$$\chi^2=\frac{1}{N-1}\sum_{i=1}^{N}\left[\frac{\sigma_{\mathrm{exp}}(\theta_i)-\sigma_{\mathrm{th}}(\theta_i)}{\Delta_{\mathrm{exp}}(\theta_i)}\right]^2. \qquad (13)$$

Here σ_{exp} and σ_{th} are the experimental and theoretical cross sections, respectively, and Δ_{exp} is the error assigned to an experimental cross section. Using χ^2 alone to evaluate goodness-of-fit can be misleading. A study of Fig. 5 will convince one that the interpolated potential (YZ) actually gives the bets prediction because of its agreement with the data at small angles. Because of the small error on the 24° point about 60% of χ^2 for potential YZ results from this single point. The conclusion is that the most reasonable potential, though by no stretch of the imagination a proper potential, results in the best agreement with experiment. The inability to properly predict the filling-in of the valley in the angular distribution near $\theta=25°$ may be due to either the poor determination of the ^{3}He optical potential, to improper treatment of the bound state function, or to the possibility of other mechanisms playing a role. This possibility will be discussed further in Sec. VB below.

The situation is equally difficult in the case of ^{3}He scattering from ^{39}K. The ^{3}He elastic data available is the scattering from ^{40}Ca at 22 MeV[42] and 37.7 MeV.[44] These potentials are given in Table II, together with an interpolated potential which will be used for all spectroscopic analysis. Figure 4(b) compares the predictions of these potentials together with the best fit deuteron potential for the K(0) reaction. The shapes of the pre-

[41] B. M. Preedom, E. Newman, and J. C. Hiebert (to be published).
[42] D. D. Arsmtrong, A. G. Blair, and R. H. Bassel (to be published).
[43] P. E. Hodgson, *The Optical Model and Elastic Scattering* (The Clarendon Press, Oxford, England, 1963); E. R. Flynn and R. H. Bassel, Phys. Letters **15**, 168 (1965); we gratefully acknowledge W. E. Burcham, D. J. Baugh, P. M. Rolph, and S. M. Scarrott of the University of Birmingham, England, for making data available prior to publication; the optical-model fits were done by the code HUNTER; W. P. Alford, L. M. Blau, and D. Cline, Nucl. Phys. **61**, 368 (1965).
[44] B. W. Ridley, E. F. Gibson, J. J. Kraushaar, M. E. Rickey, and R. H. Bassel, Bull. Am. Phys. Soc. **11**, 118 (1966), and to be published.

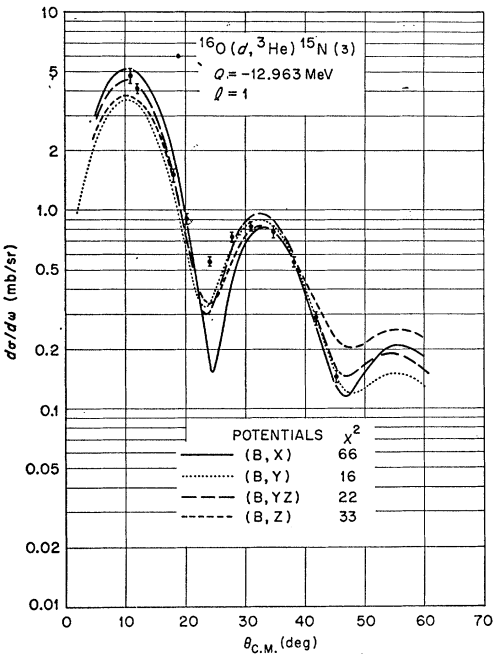

FIG. 5. Comparison of DW predictions based on ^{3}He potentials of Table II after a least-squares fit to the N(3) reaction data. Potential *YZ* results from a linear extrapolation of parameters with energy between potentials *Y* and *Z* and to the appropriate ^{3}He energy for this reaction.

dictions agree remarkably well in the region of interest, $\theta<50°$. The variation of the predicted magnitudes is to be expected from the different imaginary potentials.

C. Spin-Orbit Coupling

A comparison of the effects of spin-orbit coupling in the DW predictions is shown in Figs. 2(c), 3(c), and 4(c). All of the calculations under discussion were carried out without a lower cutoff. In each figure two comparisons are made with the standard calculation; that is the (B,X) potentials for the N(0) and N(3) reactions, and the (B,IJ) potentials for the K(0) reaction. The first comparison is made by turning off all spin-orbit coupling in the standard calculations. Thus, the bound state functions are calculated without the use of a spin-orbit potential and V_{so} is set to zero in the potentials B. These predictions are labeled "(B,X) without $\mathbf{L}\cdot\mathbf{S}$" in Figs. 2(c) and 3(c) and "(B,IJ) without $\mathbf{L}\cdot\mathbf{S}$" in Fig. 4(c). The second comparison uses potentials B' obtained from optical-model fits to the deuteron elastic-scattering data[16] in which no spin-orbit term is present in the optical potential, Eq. (12). The B' potentials are given in Table I. In no calculation has a spin-orbit potential been used in the ^{3}He channel, since as mentioned above, there is no evidence for the need of a spin-orbit term in optical potentials describing ^{3}He elastic scattering. Trial predictions have been made for the N(0) and N(3) reactions including a spin-orbit term in the ^{3}He channel of strength $V_{so}=10$ and 20 MeV. These predictions were identical in shape and magnitude to the (B,X) predictions for $\theta<40°$. Small differences do appear at larger angles but are unimportant for determining spectrosocpic factors. This effect might have to be considered, however, when attempting to determine the total angular momentum of proton states from $(d,^3\mathrm{He})$ angular distributions.

The predictions for the pickup of a $1p_{1/2}$ proton from ^{16}O, Fig. 2(c), show very little sensitivity to the omission of spin-orbit coupling from the calculation. For angles greater than 40° there are some shape differences, but these are not very strong. In particular, the potentials B and B' for ^{16}O are very similar other than the V_{so} well difference and give virtually identical predictions for the N(0) reaction. The effect on the magnitude of omitting spin-orbit coupling will be discussed below. The $1p_{3/2}$ proton pickup, the N(3) reaction in Fig. 3(c), also shows little sensitivity to the spin-orbit potentials in the shape of the angular distribution for $\theta<50°$.

The shape of the DW prediction is more sensitive to the spin-orbit term for the K(0) reaction, Fig. 4(c). The origin of this change can be traced to the 25% increase in the deuteron imaginary well depth required in fitting the elastic scattering when the spin-orbit term is turned off; compare potentials B and B'. This increased sensitivity to spin-orbit coupling with increasing A has also been observed in the optical-model study of 34.4-MeV deuteron elastic scattering.[16] The influence of the $\mathbf{L}\cdot\mathbf{S}$ coupling on the shape of the angular distribution for $\theta<50°$ is weak as was the case for the ^{16}O reactions.

D. Radial Cutoff

The effects of introducing a radial cutoff are shown in Figs. 2(d), 3(d), and 4(d). As discussed in Sec. II, the use of a sharp radial cutoff in DW calculations is physically incorrect and the smooth damping factors introduced in the LEA approximation are to be preferred. However, it is still of interest to compare the effects of radial cutoff upon the DW predictions and to demonstrate that even in the zero-range approximation the predictions without a radial cutoff more accurately reproduce the observed angular distributions.

The N(0) and N(3) reactions are shown in Figs. 2(d) and 3(d), respectively. For angles less than 40° the main effect of cutoff is a deepening of the diffraction minima, particularly for the N(3) reaction, even with an unreasonably large cutoff of 5 F. This would indicate that the contributions to the radial overlap integral from the nuclear interior are quite small. One may also see that the magnitude of the cross section in the first peak is insensitive to the use of radial cutoffs.

The K(0) reaction, Fig. 4(d), is seen to be much more sentitive to radial cutoffs. Both shape and magnitude of the predictions are strongly dependent on the cutoff used. Figure 6 shows these same predictions normalized to the first peak in the experimental angular distribution.

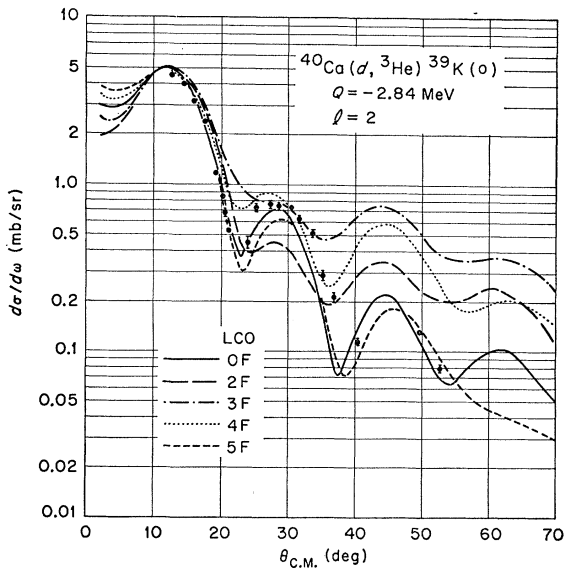

FIG. 6. Comparison between the measured cross sections and DW predictions with lower cutoffs for the K(0) reaction. Predictions have been normalized to the peak at 12° in the angular distribution.

The prediction without a cutoff results in the best fit to the data, although that with the 5-F cutoff is not too different from the no-cutoff prediction.

This striking difference in sensitivity to radial cutoff between the ^{16}O reactions and the ^{40}Ca reaction can be attributed to the ^{3}He optical potentials. The ^{39}K+^{3}He potential, potential *II* in Table II, has a shallow, diffuse imaginary term while the imaginary part of the ^{15}N potential, potential *X*, is much deeper and less diffuse. Thus, we expect the ^{3}He distorted wave to penetrate further into the nucleus in the ^{39}K case with the resultant sensitivity to radial cutoff. This expectation is borne out by displaying the radial behavior of the ^{3}He distorted waves for the two ground-state reactions in Fig. 7. This figure shows that the wave function associated with the ^{39}K(0) scattering has a strong focus in the nuclear interior, whereas this focus is nearly eliminated by the deeper absorptive well in the ^{15}N(0) scattering. However, had potential *Z* of Table II been used in place of potential *X*, the ^{15}N reaction predictions would also become extremely sensitive to radial cutoff.

The effects of using a cutoff may be investigated in greater detail by looking at the structure of the matrix element, $\beta_j{}^{lm}$ defined in Eq. (7). The quantities $\beta_j{}^{lm}$ may be defined as

$$\beta_j{}^{lm}(\theta)-\sum_L \bar{\beta}_{jL}{}^{lm}P_L{}^m(\theta)\,, \qquad (14)$$

where $P_L{}^m(\theta)$ are associated Legendre functions. In the ^{15}N(0) $l=1$ transfer there are two amplitudes contributing, with $m=0$, 1. The quantum number j can be ignored, since these amplitudes have been calculated with spin-orbit coupling omitted everywhere except in the evaluation of the bound-state function. Similarly, in the ^{39}K(0) reaction an $l=2$ transfer is considered, and thus there are three reduced amplitudes $\bar{\beta}_L{}^{2m}$ with $m=0$, 1, 2.

In Fig. 8 is shown the dependence of the largest reduced amplitudes, $m=0$, on the radial cutoff for the two ground-state reactions. The ^{15}N(0) reaction shows only a small sensitivity of $\bar{\beta}_L{}^{10}$ to cutoff, in agreement with the conclusion that the ^{3}He wave function is strongly damped in the nuclear interior and that the $(d,{}^3\mathrm{He})$ reaction must be restricted to the nuclear surface by this choice of a ^{3}He optical potential. The situation is very different in the ^{39}K(0) reaction, for which Fig. 8 shows that the 3-F lower cutoff strongly enhances the contribution of the small partial waves to the reaction. The use of a 5-F lower cutoff happens to coincide very closely with the no-cutoff reduced amplitude. This implies that destructive interference is taking place in the nuclear interior, and the use of a radial cutoff smaller than 5-F eliminates some of the interference. The result is an increase in the predicted cross section and the sensitivity of the shape of the angular distribution to the cutoff chosen. Again, it is emphasized that this sensitivity to cutoff in the ^{39}K(0) reaction and the much-reduced sensitivity in the ^{15}N(0) case is primarily due to the difference in the imaginary potentials for the ^{3}He scattering.

Thus, the conclusion as to the use of radial cutoffs in the analysis of $(d,{}^3\mathrm{He})$ reactions is the same as that for (d,p) reactions.[3] The use of an arbitrary sharp cutoff is not justified, either from a consideration of the shape of the angular distribution or the magnitude of the cross

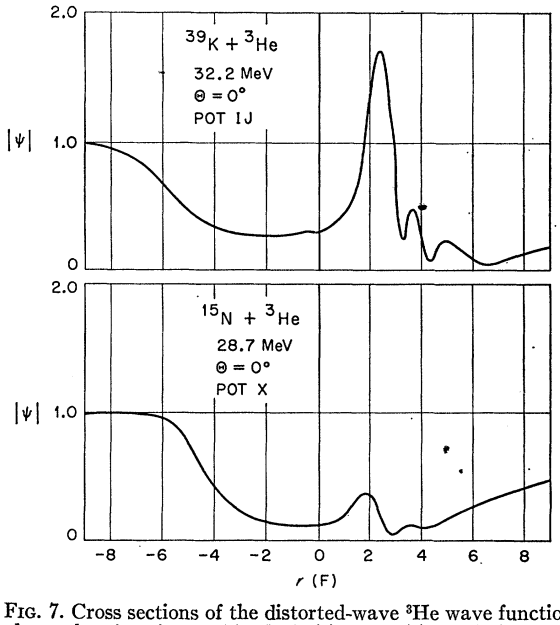

FIG. 7. Cross sections of the distorted-wave ^{3}He wave functions in the nuclear interior used in the K(0) and N(0) predictions. The cross sections were taken along the incident beam direction through the center of the nucleus with negative radii referring to the illuminated side of the nucleus, positive radii to the shadow side.

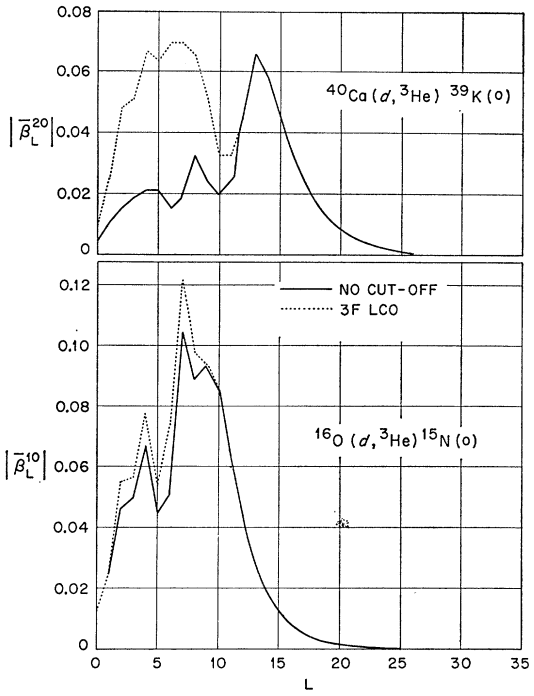

FIG. 8. Comparison between reduced amplitudes $|\bar{\beta}_L{}^{l0}|$ calculated with and without lower cutoffs for the K(0) and N(0) reactions.

section. Even though there may be cases, such as the N(0) and N(3) reactions, where the use of a cutoff does not make a substantial difference in the small angle data, and thus for the extraction of spectroscopic information, we see no reasons for using cutoffs. However, a detailed study of the large angle shape of the angular distributions and the importance of the treatment of the contributions from the nuclear interior remains to be made. It is our contention herein that most spectroscopic information can be obtained from a DW analysis of the small-angle ($\theta \lesssim 45°$) data when $E_d \approx 35$ MeV.

E. Nonlocal and Finite-Range Approximations

The nonlocal (NL) and finite-range (FR) calculations (LEA) are compared with the local zero-range approximation (LZR) in Figs. 9–11. In each of the figures the four different predictions have been normalized to the experimental data by minimizing χ^2, in Eq. (13). Values of χ^2 corresponding to the "fits" shown in the figures are given in Table III. First note from the figures that the shapes of the predicted angular distributions are not very sensitive to the type of approximation used in the calculation. This is borne out by the values of χ^2 which do not vary more than about 25%. The one exception is the prediction with both nonlocal and finite-range effects included for the N(0) reaction. Thus, we would conclude that the use of nonlocal and/or finite-range corrections does not lead to any improvement in the shape of the predicted angular distributions for these reactions.

TABLE III. Comparison of DW predictions.

	LZR		NL		FR		NL+FR	
Final State	χ^2	C^2S	χ^2	C^2S	χ^2	C^2S	χ^2	C^2S
N(0)	31	2.28	41	1.61	42	2.12	98	1.51
N(3)	67	3.61	77	2.87	47	3.69	57	2.93
N(0)	24	4.98	32	3.53	29	4.23	31	3.21

This result is in contrast with that reported by Bassel[20] for the ^{48}Ca(^{3}He,d)^{49}Sc ground-state reaction at 22 MeV. In that study, the inclusion of nonlocal and finite-range effects resulted in a strong suppression of the large-angle cross sections and a consequent improvement in the agreement between experiment and theory. Bassel attributes this effect both to suppression of the interior and also to enhancement of the form factor at

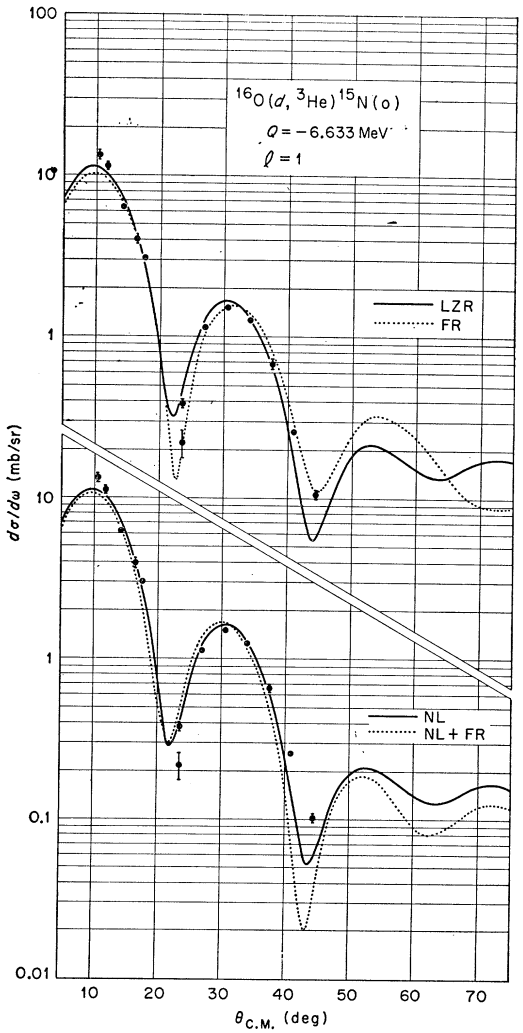

FIG. 9. Comparison between the experimental cross section and the DW predictions based on zero-range, nonlocal, and finite-range calculations with spin-orbit coupling for the N(0) reaction. The predictions have been least-squares fit to the data with resulting spectroscopic factors and χ^2 values shown in Table III.

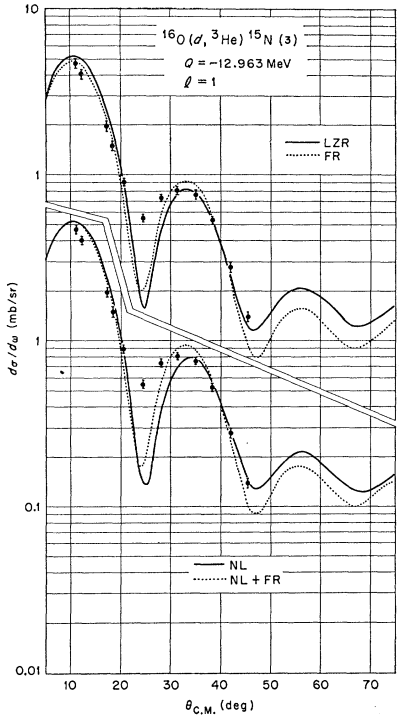

FIG. 10. Comparison between the experimental cross sections and the DW predictions based on zero-range, nonlocal, and finite-range calculations with spin-orbit coupling for the N(3) reaction. The predictions have been least-squares fit to the data with resulting spectroscopic factors and χ^2 values shown in Table III.

large radii. It has been suggested[45] that the nonlocal and finite-range effects would produce a much broader radial form factor for the 22-MeV reaction, thus predicting a more rapid decrease of cross section with angle. This is because the focus of the optical-model wave function would be moved closer to the center of the nucleus by the nonlocal and finite-range corrections as the channel energy is reduced. Thus, the radial overlap of the distorted waves with the bound-state function results in a broader form factor as the foci move in and the bound-state function moves out. This effect is further enhanced since the 22-MeV reaction deals with a $1f_{7/2}$ orbital which peaks at a larger radius than the $1p$ or $1d$ orbitals. For the reactions considered herein, the distorted-wave foci occur slightly outside the bound-state-function peaks; thus the smaller movement toward the center of the nucleus due to the corrections appears to have little effect on the radial overlap. A careful study of the details of these predictions will be required to determine the reasons for the striking differences at 22 and 32 MeV (equivalent ^{3}He energies).

F. Spectroscopic Factors

The least-squares fits of the DW predictions to the experimental angular distributions shown in Figs. 9–11 result in the spectroscopic factors tabulated in Table III. For the present discussion, it is assumed that the two-particle, two-hole ground-state correlations are small in the ^{16}O and ^{40}Ca nuclei, and thus the spectroscopic factors should approximate the shell-model predictions: $C^2S=2$ for the N(0) reaction and $C^2S=4$ for both the N(3) and K(0) reactions. The local zero-range and finite-range calculations result in spectroscopic factors within about 10% of the shell-model values for the ^{15}N states. In the K(0) reaction the local zero-range result is 25% larger, while the finite-range C^2S is only 5% larger than the shell-model value. The nonlocal calculations, both in zero-range and finite-range, tend to underestimate the spectroscopic factors by 20–30% for all three reactions. The difficulty with these nonlocal predictions probably arises in our lack of knowledge about the energy dependence of the shell-model potential. It has been noted that this energy dependence may not be as strong for particles near the top of the Fermi sea as it is for deeply bound orbitals or continuum wave functions.[46] Studies with other nuclear reactions[45] suggest that nonlocality should only be used in the scattered wave functions and not in the bound-state functions. These same difficulties with the nonlocality effects were noted in the ^{48}Ca-$(^3\mathrm{He},d)^{49}$Sc study.[20]

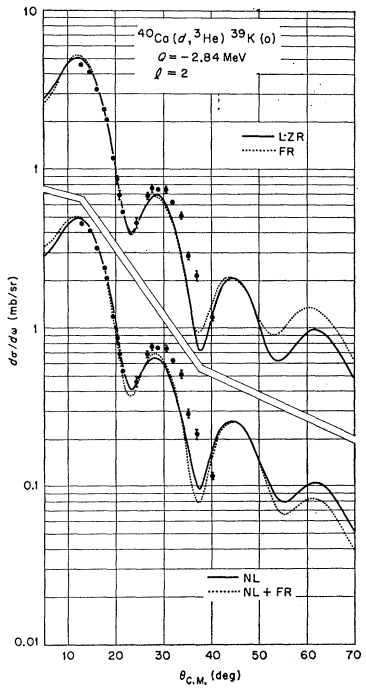

FIG. 11. Comparison between the experimental cross sections and the DW predictions based on zero-range, nonlocal, and finite-range calculations with spin-orbit coupling for the K(0) reaction. The predictions have been least-squares fit to the data with resulting spectroscopic factors and χ^2 values shown in Table III.

[45] R. M. Drisko (private communication).

[46] G. E. Brown, J. H. Gunn, and P. Gould, Nucl. Phys. **46**, 598 (1963); G. R. Satchler (private communication).

TABLE IV. Corrections to peak cross sections required for agreement with the local zero-range predictions of the "best" potentials.

Reaction	Potentials[a]	No cutoff	3 F Cutoff	5 F Cutoff
^{15}N(0)	(*B*,*X*)	0%	+4%	+6%
	(*B*,*X*) without spin-orbit coupling	−10%	−6%	−7%
	(*A*,*X*)	−1%	+3%	+4%
	(*B*,*Y*)	+39%	+46%	+22%
	(*B*,*Z*)	+9%	+20%	+3%
^{15}N(3)	(*B*,*X*)	0%	+6%	+7%
	(*B*,*X*) without spin-orbit coupling	+13%	+21%	+21%
	(*A*,*X*)	−2%	+2%	+5%
	(*B*,*Y*)	+30%	+38%	+14%
	(*B*,*YZ*)	+5%	+13%	−1%
	(*B*,*Z*)	+1%	+19%	+4%
^{39}K(0)	(*B*,*IJ*)	0%	−13%	−10%
	(*B*,*IJ*) without spin-orbit coupling	−18%	−28%	−24%
	(*A*,*IJ*)	−5%	−11%	−17%
	(*B*,*I*)	+19%	+5%	+8%
	(*B*,*J*)	−18%	−27%	−26%

[a] The potentials are listed in Tables I and II. The abbreviation (*B*,*X*) refers to the use of deuteron optical-potential *B* in the incident channel and ^{3}He optical-potential *X* in the exit channel.

One of the encouraging features of Table III is the rather good agreement between the spectroscopic factors resulting from the local zero-range and finite-range predictions. The largest discrepancy is 18% in the K(0) case. Although the finite-range calculation is to be preferred, these results and the ^{40}Ca(d,^{3}He) reactions reported below indicate that the zero-range predictions are acceptable and yield values of C^2S which are 10–20% larger than the corresponding finite-range predictions. The only strong exception to this conclusion is the N(3) reaction which is subject to other uncertainties, as discussed below.

A second, and perhaps more important point, is that the DW theory is predicting the proper magnitudes for the (d,^{3}He) cross sections in the 25–35 MeV region of incident deuteron energies when the local form of the theory is used. Thus, the (d,^{3}He) and (^{3}He,d) reactions can be used to investigate the nature of proton-hole and proton-particle states with the expectation of extracting fairly reliable spectroscopic information concerning these states.

Table IV indicates roughly the variation in the predicted cross sections, and thus spectroscopic factors, which result from the various potentials discussed above. In this table are compared the cross sections of the first peak of the angular distributions relative to the predictions of the "best" potentials available. These "best" potentials are the first set listed in the table for each reaction and are the potentials used in extracting all spectroscopic factors.

Note that the average deuteron potentials (*A*) require only a small (1–5%) adjustment to reproduce the predictions of the best (*B*) deuteron potentials. The predictions of the various ^{3}He optical potentials vary significantly and point up the need for a thorough study of ^{3}He scattering as a function of both target nucleus and ^{3}He energy. It is also evident that the introduction of a lower cutoff has a large effect on cross-section magnitudes. Thus, from both the shape and magnitude effects we argue against the use of cutoffs in the use of the DW theory for these reactions.

Table IV also shows that predictions that do not include spin-orbit coupling should be renormalized by about $\pm 10\%$ for $j=l\pm\frac{1}{2}$ with $l=1$ and by about $\pm 20\%$ for $l=2$. These numbers can be used only as rough guides since the correction is sensitive to the binding energy of the orbital under consideration. It should be pointed out that these numbers apply only to local zero-range calculations with no cutoff.

V. NUCLEAR STRUCTURE

In the discussions that follow concerning the nuclear-structure information resulting from the present (d,^{3}He) study, we shall take the point of view that the local finite-range form of the DW theory gives the most

TABLE V. Spectroscopic factors from ^{16}O(d,^{3}He)^{15}N.

^{15}N level (MeV)	Assumed proton configuration	LZR	C^2S NL	FR
G.S.	$(1p_{1/2})^{-1}$	2.30	1.87	2.14
5.28	$(1p)^{-2}(1d_{5/2})^1$	0.31	0.24	0.31
5.30	$(1p)^{-2}(2s_{1/2})^1$	0.038	0.016	0.039
6.33	$(1p_{3/2})^{-1}$	3.64	3.32	3.72
ΣC^2S		6.0	6.29	5.40	6.21

TABLE VI. Spectroscopic factors from ^{40}Ca(d,^{3}He)^{39}K.

^{39}K level (MeV)	Configuration	LZR	C^2S NL	FR
0	$(1d_{3/2})^{-1}$	4.98	3.53	4.23
2.53	$(2s_{1/2})^{-1}$	1.93	1.35	1.62
2.82	$(2s,1d)^{-2}(1f_{7/2})^1$	0.50	0.45	0.46
3.02	$(2s,1d)^{-2}(2p_{3/2})^1$	0.045	0.038	0.044
4.14	$(2s_{1/2})^{-1}$	0.19	0.12	0.17
5.32	$(1d_{5/2})^{-1}$	1.33	0.98	1.09
5.75	$(1d_{5/2})^{-1}$	0.85	0.66	0.68
6.67	$(1d_{5/2})^{-1}$	1.65	1.31	1.26
7.47	$(1d_{5/2})^{-1}$	0.35	0.29	0.26
8.09	$(1d_{5/2})^{-1}$	0.66	0.56	0.50

reliable spectroscopic information. For comparison purposes, the corresponding values of C^2S using the zero-range and nonlocal forms of the theory are shown in the tables. The spectroscopic factors extracted for the ^{15}N and ^{39}K levels studied are presented in Tables V and VI, respectively.

A. ^{15}N Ground State

The major part of the ^{15}N ground-state wave function is certainly a $p_{1/2}$ hole coupled to the ^{16}O ground state. Even though the ^{16}O ground state may not be a closed-shell state (to be discussed below), the overlap between the possible 2-particle–2-hole (2p-2h) and 4-particle–4-hole (4p-4h) configurations in the ^{16}O and ^{15}N ground states is presumably quite good. Another possible configuration in the ^{15}N ground state is $|\{(p_{3/2})^{-1},2^+\}\frac{1}{2}^-\rangle$. This is expected to be quite small because of the large $p_{3/2}$-$p_{1/2}$ splitting (6–8 MeV). Furthermore, this component of the ^{15}N ground-state configuration could only be reached through a two-step process, core excitation plus pickup, with the $(d,{}^3\mathrm{He})$ reaction. Therefore, this reaction is expected to proceed via the pickup of a $1p_{1/2}$ proton, and the resultant spectroscopic factor of 2.14 is in good agreement with the shell-model prediction of 2.0.

B. The $\frac{3}{2}^-$ State at 6.33 MeV in ^{15}N

This state and its mirror state in ^{15}O at 6.18 MeV have been the subject of considerable discussion recently. Rose and Lopes[47] conjecture that the configuration of this state is a superposition of the $\frac{3}{2}^-$ hole coupled to the ground state of ^{16}O and a $\frac{1}{2}^-$ hole coupled to the excited 2^+ state of ^{16}O, i.e.,

$$|\tfrac{3}{2}^-\rangle = a|\{(p_{3/2})^{-1},0^+\}\tfrac{3}{2}^-\rangle + b|\{(p_{1/2})^{-1},2^+\}\tfrac{3}{2}^-\rangle.$$

They further suggest that the $\frac{3}{2}^-$ state in ^{15}N at 9.16-MeV excitation is the orthogonal combination of these basic states. Our analysis of the $(d,{}^3\mathrm{He})$ transition to the 6.33-MeV state, assuming a $p_{3/2}$ pickup, results in a spectroscopic factor of 3.72, which is in close agreement with the shell model. This deviation from the shell model, while within the uncertainty of the theory, is probably significant and may, in part, be due to the admixture of the excited core configuration discussed above.

A brief search for the 9.16-MeV level showed no cross section greater than 15% of that for the 6.33-MeV level. Similar results have been reported for the mirror states in ^{15}O through studies with the ^{16}O$(^3\mathrm{He},\alpha)^{15}$O reaction at 31 MeV[48] and the ^{16}O$(p,d)^{15}$O reaction at 41 MeV.[49]

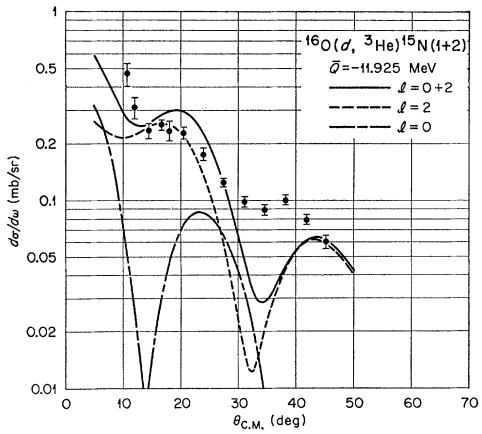

FIG. 12. Angular distribution for the ^{16}O$(d,{}^3\mathrm{He})$ reactions to the unresolved first and second excited states in ^{15}N. The solid curve results from optimizing the contributions of $l=0$ and $l=2$ zero-range DW predictions by a least-squares method. The dashed curves indicate the individual $l=0$ and $l=2$ contributions.

Thus, we conclude that the 6.33-MeV level is primarily a $p_{3/2}$ hole state in agreement with recent findings of Brink and Rose[50] and in disagreement with the proposal of Rose and Lopes. As discussed above, we cannot rule out a small admixture of the $|\{(p_{1/2})^{-1},2^+\}\frac{3}{2}^-\rangle$ component in this state. It is also possible that some effects of core excitation are seen in the angular distribution, Fig. 10. Evidence for the two-step mechanism has been found in the ^{12}C$(d,{}^3\mathrm{He})^{11}$C and ^{12}C$(d,t)^{11}$B reactions initiated by 50-MeV deuterons.[51] Similar results seem to be present in the ^{12}C$(d,{}^3\mathrm{He})$ reaction at 34 MeV, based on preliminary data of the present authors. These "measured" core-excitation angular distributions are rather flat and a similar mechanism may be contributing to the filling of the first minimum of the angular distribution shown in Fig. 11. This is only one possibility, since the filling of the minimum may be simply a Q effect not properly accounted for in our treatment of the DW theory.

C. The $\frac{5}{2}^+$, $\frac{1}{2}^+$ Doublet at 5.3 MeV in ^{15}N

The observed angular distribution for the reactions proceeding to the unresolved $\frac{5}{2}^+$ level at 5.270 MeV and $\frac{1}{2}^+$ level at 5.299 MeV in ^{15}N is shown in Fig. 12. The observation of these states is interpreted as evidence for the presence of $(1s)^4(1p)^{10}(2s,1d)^2$ and/or $(1s)^4(1p)^8$-$(2s,1d)^4$ configurations in the ground state of ^{16}O. This interpretation is by no means the only possible one since core excitation could be responsible for a part of this cross section. If simple proton pickup is the only reaction mechanism, a further problem occurs in the extraction of spectroscopic information, since we do not know how to deal properly with the bound-state functions for

[47] H. J. Rose, and J. S. Lopes, Phys. Letters **18**, 130 (1965); J. S. Lopes, O. Hausser, H. J. Rose, A. R. Poletti, and M. F. Thomas, Nucl. Phys. **76**, 223 (1966).
[48] E. K. Warburton, P. D. Parker, and P. F. Donovan, Phys. Letters **19**, 397 (1965).
[49] J. B. Marion, C. A. Ludemann, and P. G. Roos, Bull. Am. Phys. Soc. **11**, 332 (1966); and Phys. Rev. (to be published).
[50] D. M. Brink and H. J. Rose (to be published).
[51] M. Chabre, D. L. Hendrie, H. G. Pugh, and C. Detraz, Bull. Am. Phys. Soc. **11**, 317 (1966).

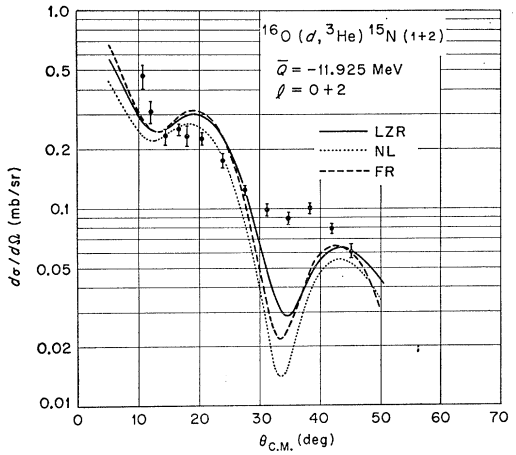

FIG. 13. Comparison between the experimental cross section and DW predictions based on zero-range, nonlocal, and finite-range calculations with spin-orbit coupling for the N(1+2) reactions. The $l=0$ and $l=2$ contributions have been determined by the least-squares method with the resulting spectroscopic factors shown in Table V.

($2p$-$2h$) and ($4p$-$4h$) states. We begin with the results of the above interpretation of the data and then consider these other difficulties.

In the above interpretation of these reactions a $1d_{5/2}$ proton is picked up from the ^{16}O ground state, leaving the residual ^{15}N nucleus in the $\frac{5}{2}^+$ state at 5.270 MeV. This component of the angular distribution is indicated by the dashed line in Fig. 12. Similarly, a $2s_{1/2}$ proton is picked up, populating the $\frac{1}{2}^+$ level at 5.299 MeV. This state is characterized by the $l=0$ shape indicated by the dot-dashed line in the figure. The solid curve in Fig. 12 is the result of adding the two components, using a least-squares method to best reproduce the experimental data. The DW predictions in Fig. 12 are local zero-range calculations which use the B_{sep} prescription for determining binding energies. Figure 13 compares the nonlocal and finite-range (LEA) predictions with the zero-range calculation. Spectroscopic factors resulting from these comparisons to experiment are shown in Table V.

To verify the DW predictions for the shape of angular distributions for $l=0$ and $l=2$ orbital pickup reaction, data has been taken for the ^{19}F(d,^{3}He)^{18}O reaction at 34.4 MeV.[52] A comparison of the pertinent data and the corresponding DW predictions is shown in Fig. 14. The DW predictions were made using the average deuteron potential for ^{19}F based on Ref. 16 and the 29-MeV ^{3}He+^{16}O potential, potential Z of Table II. The agreement between experiment and theory in Fig. 14 is quite good, indicating that $l=0$ and $l=2$ predictions should be reasonably accurate in this region of A. We are presently measuring the ^{16}O(d,t)^{15}O angular distributions for the reactions proceeding to the mirror states, attempting to resolve the two states and look at the $l=0$ and $l=2$ angular distributions directly. This study should clear up some of the questionable points in the analysis of the present data.

Previous studies have raised the possibility of the $\frac{1}{2}^+$ mirror states in ^{15}O and ^{15}N having a $(1s)^3(1p)^{12}$ admixture.[48,53] The present analysis indicates that the

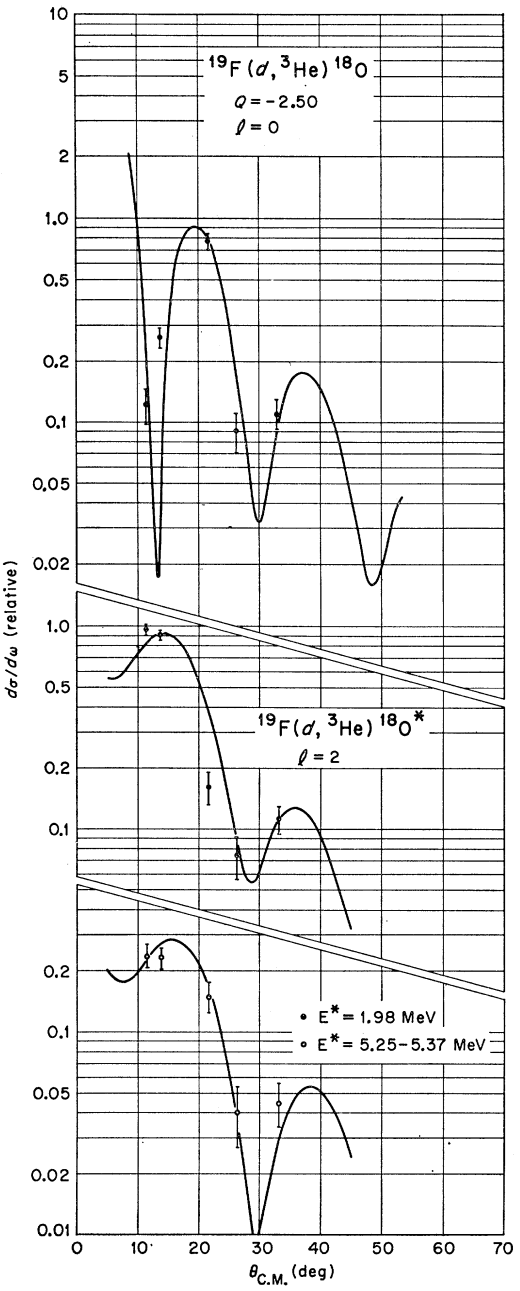

FIG. 14. Angular distributions for $l=0$ and $l=2$ pickup reactions ^{19}F(d,^{3}He)^{18}O. Solid curves are predictions for the appropriate reactions.

[52] M. R. Cates, J. C. Hiebert, and E. Newman (to be published).

[53] K. J. Foley, G. L. Salmon, and A. B. Clegg, Nucl. Phys. **31**, 43 (1962).

contribution from this configuration is quite unlikely, since an unreasonably large $C^2S(1s)=0.3$ results from this assumption. The intermediate coupling calculations of Halbert and French,[54] which agree well with the experimental evidence on the low-lying even parity levels of ^{15}N, also indicate very small admixtures of the $(1s)^3(1p)^{12}$ in the lowest levels.

The evidence for $(2p$-$2h)$ and/or $(4p$-$4h)$ configurations in the ^{16}O ground state agree qualitatively with recent theoretical work on the ^{16}O ground state. A shell-model calculation[55] using three different two-body forces results in large $(2p$-$2h)$ admixtures, varying from 21%-47% of the ground-state wave function. Similarly, a calculation[56] mixing low-lying deformed states and shell-model states results in 22% $(2p$-$2h)$ and about 2% $(4p$-$4h)$ configurations in the ^{16}O ground state. A part of the $(2p$-$2h)$ strength leading to states above the third excited state in ^{15}N may have been missed. A preliminary search for evidence of the population of such higher excited states at a laboratory angle of 34° revealed a state near 8.5 MeV in ^{15}N with 21% of the 6.33-MeV state yield.

The extraction of reliable spectroscopic factors in reactions involving $(2p$-$2h)$ configurations is exceedingly difficult due to our lack of knowledge of the radial dependence of these wave functions. In these cases the effective binding energy B_{eff} would seem to be a reasonable approximation. Here the same potential well ($V=62$ MeV) that is appropriate for the $1p_{1/2}$ orbital is used to bind the $1d_{5/2}$ and $2s_{1/2}$ particles. This prescription admittedly does not include the contribution

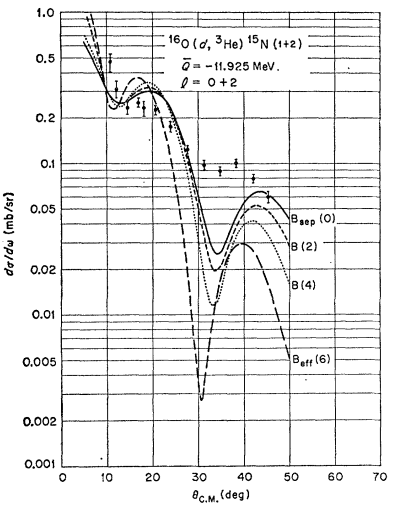

FIG. 15. Comparison between the experimental cross sections and DW predictions for the N(1+2) reactions as a function of binding energies, varied in equal steps between B_{sep} and B_{eff}. The $l=0$ and $l=2$ contributions were determined by the least-squares method.

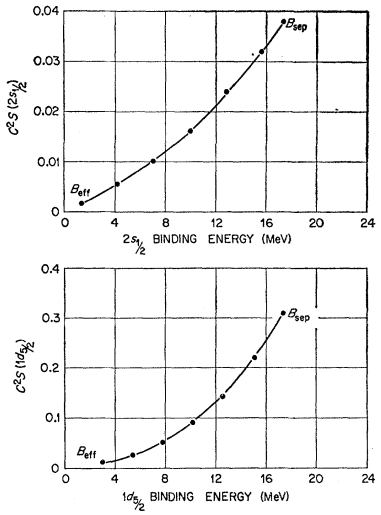

FIG. 16. Variation of $1d_{5/2}$ and $2s_{1/2}$ spectroscopic factors with assumed binding energies in equal steps between B_{sep} and B_{eff}.

to the binding from the pairing energies and thus underestimates the binding. Consequently, we have calculated the mixing of $l=0$ and $l=2$ contributions to the ^{15}N doublet reactions in a series of equal steps between B_{eff} and B_{sep}. Figure 15 shows the results of least-squares fits of $l=0$ and $l=2$ DW predictions to the experimental data as the binding energies are varied. The resulting spectroscopic factors, as a function of binding energy, are indicated in Fig. 16. It is apparent that B_{sep} results in the best agreement between the theoretical and experimental angular distributions, with the agreement becoming progressively worse as the binding energies are reduced. We do not argue from this, however, that B_{sep} is the proper prescription, since core excitation may be playing an important role in these reactions. It does seem proper to observe, from Fig. 16, that the spectroscopic factors quoted in Table V represent upper limits on the $1d_{5/2}$ and $2s_{1/2}$ admixtures in the ^{16}O ground state.

The second major difficulty in analyzing these two reactions is in determining the reaction mechanism, or mechanisms, involved. The possibility of core excitation in stripping and pickup reactions has been raised in recent theoretical[57,58] and experimental[51,59] investigations. In particular, the 50-MeV ^{12}C$(d,{}^3$He) data[51] has resulted in strong evidence for the core-excitation mechanism in that reaction. If $(2p$-$2h)$ and $(4p$-$4h)$ configurations are indeed mixed strongly in the ^{16}O ground state, there is every reason to believe that core excitation will also contribute to these reactions. At present, it is not clear whether the two-step and one-step reactions will be identifiable through characteristic angular distribu-

[54] E. C. Halbert and J. B. French, Phys. Rev. **105**, 1563 (1957).
[55] S. S. M. Wong, Phys. Letters **20**, 188 (1966).
[56] G. E. Brown and A. M. Green, Nucl. Phys. **75**, 401 (1966).
[57] S. K. Penny and G. R. Satchler, Nucl. Phys. **53**, 145 (1964).
[58] B. Kozlowsky and A. de-Shalit, Nucl. Phys. **77**, 215 (1966).
[59] R. Bock, H. H. Duhm, R. Rudel, and R. Stock, Phys. Letters **13**, 151 (1964).

tions. The model of Kozlowsky and de-Shalit,[58] applied to the ^{62}Ni(d,^{3}He)^{63}Cu reaction, indicates that the angular distributions for the two mechanisms are very similar. This is in contrast to a similar calculation carried out at Oak Ridge,[60] which predicts an angular distribution for the two-step reaction that has less structure and a slower decrease with angle. The data of Chabre *et al.*[51] are in good agreement with the latter predictions, and thus is suggestive of the characteristic shape of two-step stripping reactions. It is conceivable that these questions cannot be resolved until coupled-channel-calculations are undertaken for core-excitation stripping and pickup reactions. However, we should point out again that the failure to fit the experimental data in the region $\theta_{c.m.}=30°-40°$ might be resulting from a lack of knowledge of the ^{3}He scattering, as well as a competing reaction mechanism. In fact, a prediction using ^{3}He potential Y of Table II results in much improved agreement between experiment and theory in the shape of $d\sigma/d\Omega$ with substantially the same spectroscopic factors.

It is hoped that the continuing experimental investigation of the higher excited states in ^{15}N and a study of the ^{16}O(d,t)^{15}O reactions proceeding to the resolved mirror states in ^{15}O will resolve some of the above questions. We believe that the present evidence for the presence of $(2s,1d)^2$ configurations in the ^{16}O ground state is quite strong, and the indicated spectroscopic factors represent upper limits.

D. ^{40}Ca(d,^{3}He)^{39}K Reactions

l=2 Reactions

The ground-state angular distribution of Fig. 11 was considered in Secs. IVE and F above. The spectroscopic factors resulting from our analysis of this and all other observed states in ^{39}K are shown in Table VI. Again all reference to values of C^2S below will pertain to the finite-range form of the theory. Five additional states were observed which show $l=2$ angular distributions, ranging in excitation from 5.32 to 8.09 MeV in ^{39}K, Fig. 17. These states are assumed to result from the pickup of a $1d_{5/2}$ proton from the ^{40}Ca core. Since the sum of the observed $1d_{5/2}$ spectroscopic factors is 3.79, whereas the shell-model prediction is 6, the expectation is that other $1d_{5/2}$ hole states are located above $E^*=8.09$ MeV in ^{39}K. These states were not observed because of the experimental limitations.

The center of gravity of the observed $(1d_{5/2})$ hole states is given by

$$\bar{E}^*=\sum_i (C^2S)_i E^*_i/\sum_i (C^2S)_i=6.6 \text{ MeV}.$$

This lower limit on the location of the $1d_{5/2}$ hole strength is to be compared with the value of 6.6±1.0 MeV determined by (p,$2p$) reaction studies on ^{40}Ca.[61] The (p,$2p$) results also indicate the possibility of additional $1d_{5/2}$ hole strength at an excitation energy of about 10.5 MeV in ^{39}K. This interpretation is certainly in agreement with the fact that the observed states do not exhaust the $1d_{5/2}$ strength.

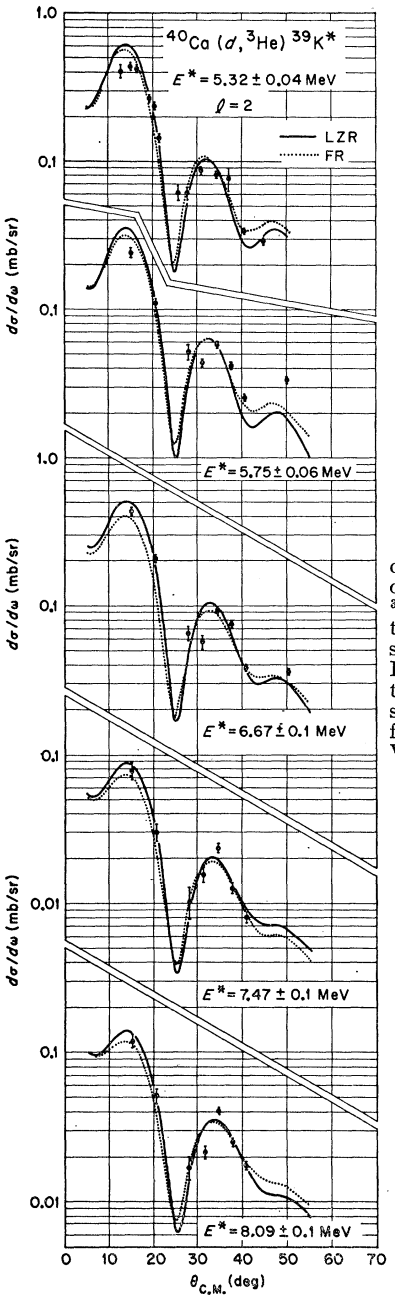

FIG. 17. Angular distributions for the observed ^{40}Ca(d,^{3}He)-^{39}K excited-state reactions with an $l=2$ shape. The curves are DW predictions fit to the data with the resulting spectroscopic factors listed in Table VI.

l=0 Reactions

Two $l=0$ angular distributions have been observed in the present study, Fig. 18. These reactions proceed to the first excited state in ^{39}K at 2.52 MeV and a state at 4.14±0.05 MeV. These states are thus in all proba-

[60] G. R. Satchler (private communication).
[61] M. Riou, Rev. Mod. Phys. **37**, 375 (1965).

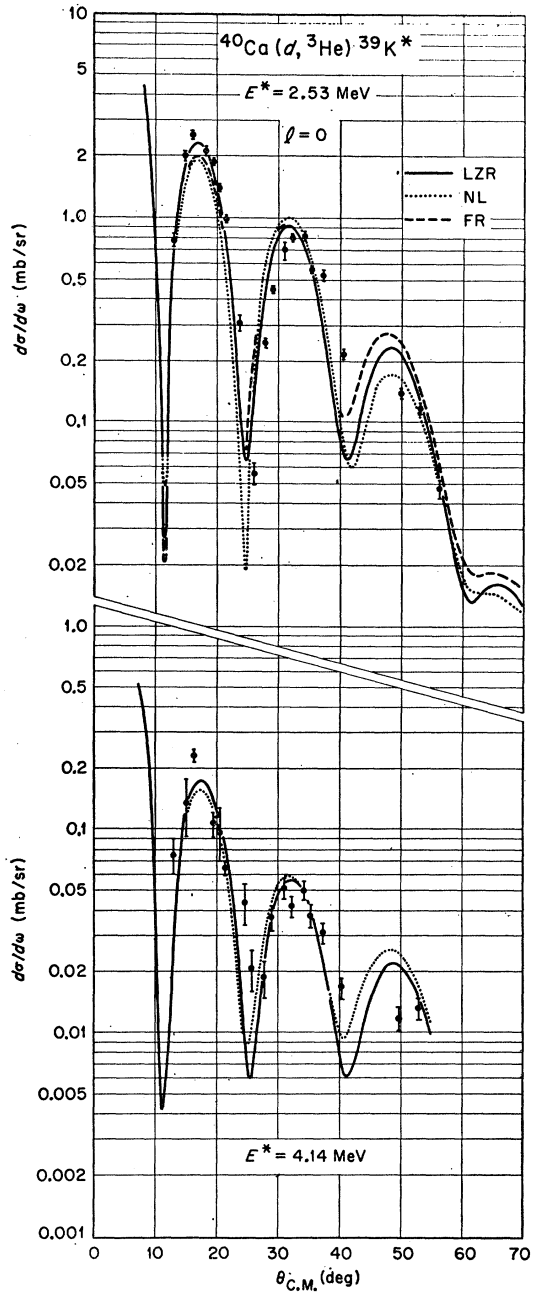

FIG. 18. Angular distributions for the observed $^{40}Ca(d,^3He)^{39}K$ excited-state reactions with an $l=0$ shape. The curves are DW predictions fit to the data with the resulting spectroscopic factors listed in Table VI.

bility $2s_{1/2}$ hole states with $J^\pi=\frac{1}{2}^+$. The sum of the spectroscopic strength for these two states is 1.79, well within the assumed 20% accuracy of our analysis and the shell-model prediction of 2.0. However, if the interpretation of the reactions proceeding to the second and third excited states of ^{39}K is correct and the ^{40}Ca nucleus has both $(2s,1d)^{-2}(1f_{7/2})^2$ and $(2s,1d)^{-2}(2p_{3/2})^2$ configurations in the ground state, then it might be expected that a third $2s_{1/2}$ hole state exists in ^{39}K and has not yet been observed. A $\frac{1}{2}^+$ state has been observed in the mirror nucleus ^{39}K at 4.04 MeV,[12,62] presumably the analog of the 4.14-MeV state observed herein.

The $\frac{7}{2}^-$ State at 2.82 MeV in ^{39}K

Figure 19 shows the measured angular distribution for the $(d,^3He)$ reaction leaving ^{39}K in its second excited state. Various investigators have recently studied the mirror state in ^{39}Ca at 2.80 MeV with (p,d) [11] and $(^3He,\alpha)$ [12,13] reactions on ^{40}Ca and have assigned $J^\pi=\frac{7}{2}^-$ to this state. The present results are in good agreement with an $l=3$ pickup, as predicted by the DW theory. This reaction gives an opportunity to test the two extreme prescriptions for the binding energy of the picked-up proton, B_{sep} and B_{eff}. In Fig. 19 are compared the DW predictions using the two prescriptions for binding energy with the zero-range, nonlocal, and finite-range forms of the theory. In each calculation the use of B_{sep} results in better agreement between theory and experiment, as indicated by the values of χ^2 which are from 2–5 times smaller than the corresponding B_{eff} predictions. This result is in direct contrast to the corresponding $^{40}Ca(p,d)^{39}Ca$ reaction to the $\frac{7}{2}^-$ state at 2.80 MeV.[11] This discrepancy between (p,d) reactions and $(d,^3He)$ reactions is perhaps due to the fact that the latter reactions are more confined to the surface[7] than the (p,d) reactions. Obviously, this question needs further experimental and theoretical study.

In this analysis $B_{eff}=3.5$ MeV and $C^2S=0.81$ with the least-squares fit shown in Fig. 19(c) or $C^2S=0.055$ if theory and experiment are matched in the first peak of the angular distribution. Thus, as was true in the ^{16}O reaction above, the values of C^2S quoted for the 2.82-MeV state in ^{39}K in Table VI represent upper limits. We note that using B_{sep} the local zero-range (LZR) value of $C^2S=0.50$ is in good agreement with the $(^3He,\alpha)$ measurement[12] to the mirror state in ^{39}Ca, which resulted in $C^2S=0.53$.

The 3.02-MeV State in ^{39}K

The measured angular distribution for the transition to the 3.02-MeV state is shown in Fig. 20, together with $l=1$ DW predictions. These data were difficult to extract due to the much larger cross section for the 2.82-MeV final-state reaction. The assignment of the orbital angular momentum of the picked-up proton is not nearly as conclusive as in the other reactions studied. However, an $l=1$ prediction certainly gives the best fit to the observed angular distribution, and we can tentatively assign $J^\pi=(\frac{1}{2},\frac{3}{2})^-$ to this state. This assignment agrees with the $(^3He,\alpha)$ results between 8 and 10.5 MeV[13] but not with a possible $l=2$ assignment made by Bock *et al.*[12] from their 18-MeV data.

[62] C. D. Kavoloski, G. Bassani, and N. M. Hintz, Phys. Rev. 132, 813 (1963).

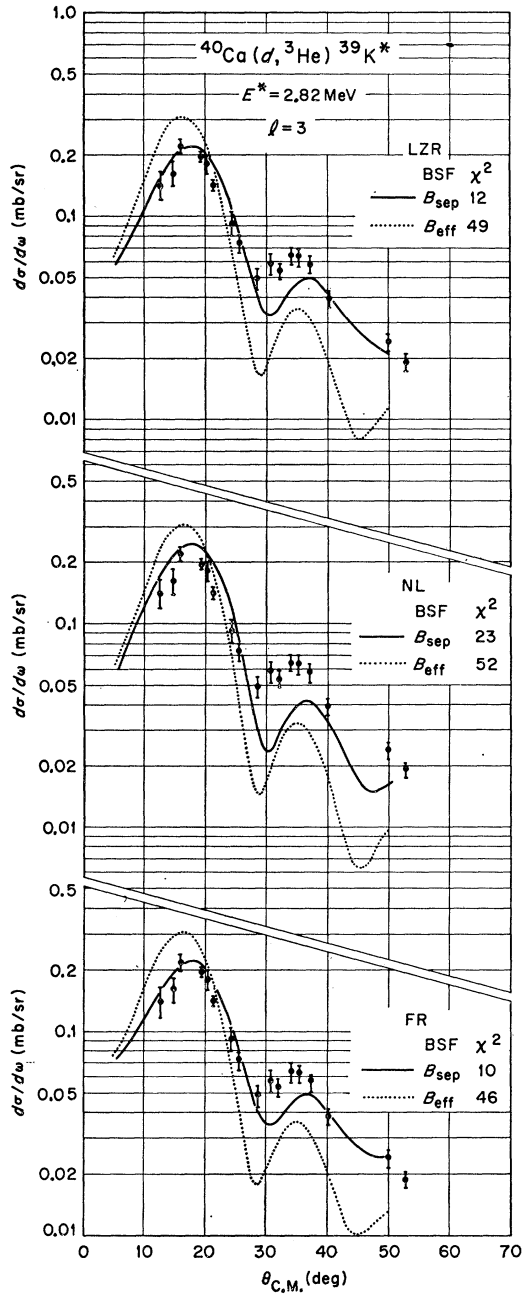

FIG. 19. Angular distribution for the ^{40}Ca(d,^{3}He) reaction populating the 2nd excited state in ^{39}K. The curves are $l=3$ predictions comparing the B_{sep} and B_{eff} prescriptions for determining the proton binding energy in ^{40}Ca, as calculated by the (a) local zero-range, (b) nonlocal, and (c) finite-range methods.

Accepting an $l=1$ assignment, it may be argued that we are observing the pickup of $2p$ protons rather than $1p$ protons. Since the observed $1d_{5/2}$ strength is centered at 6.6 MeV in ^{39}Ca, it is unlikely that there is any $1p$ strength at 3-MeV excitation. A further assumption is that the $(2s,1d)^{-2}(2p_{3/2})^2$ configuration in ^{40}Ca is the parent configuration in this reaction. This seems reasonable since the $2p_{3/2}-2p_{1/2}$ splitting is about 2 MeV in ^{41}Ca. The spectroscopic factors quoted in Table VI are based on the assumption of $2p_{3/2}$ proton pickup from ^{40}Ca to the third excited state of ^{39}K.

Figure 20 also compares the DW predictions based on B_{sep} and B_{eff}. In this case the data are not good enough to make any definite statements on these two

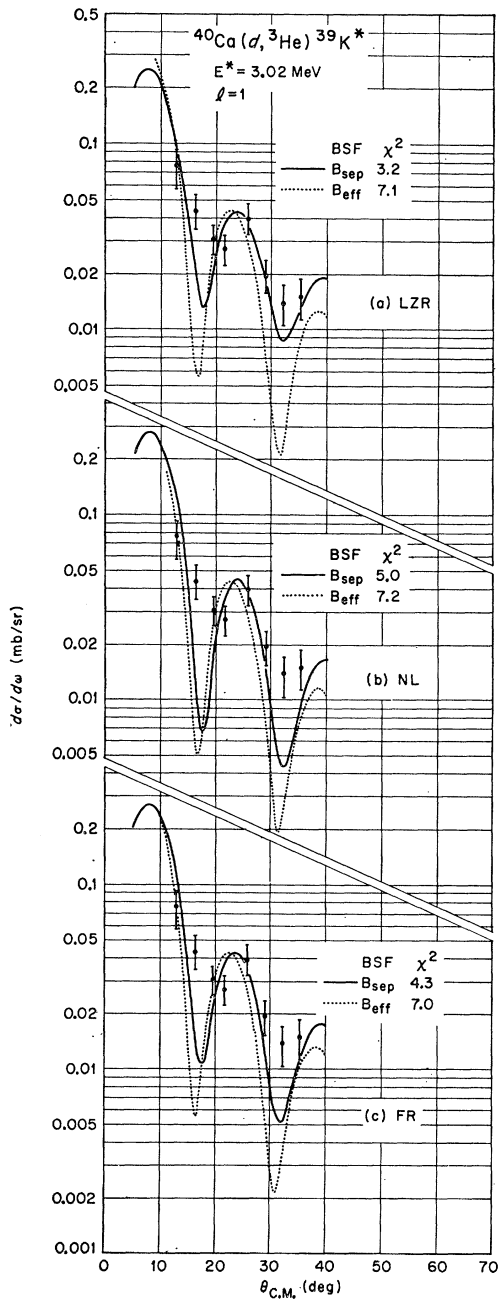

FIG. 20. Angular distribution for the ^{40}Ca(d,^{3}He) reaction populating the 3rd excited state in ^{39}K. The curves are $l=1$ predictions comparing the B_{sep} and B_{eff} prescriptions for determining the proton binding energy in ^{40}Ca, as calculated by the (a) local zero-range, (b) nonlocal, and (c) finite-range methods.

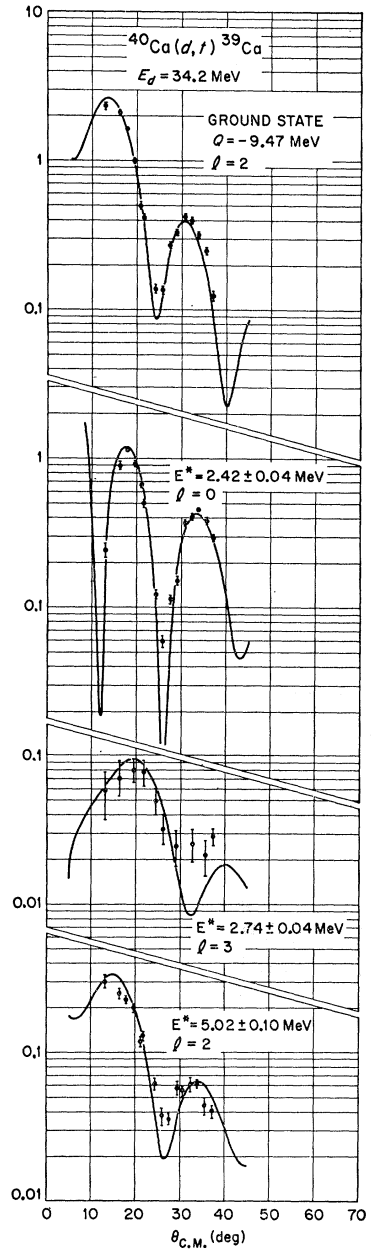

FIG. 21. Angular distributions for the observed ^{40}Ca(d,t)-^{39}Ca reactions. The solid curves are DW predictions using the same optical potentials (B,IJ) as in the ^{40}Ca$(d,{}^3\mathrm{He})$ predictions. Spectroscopic factors are shown in Table VII.

prescriptions. The separation-energy prescription does again seem to be in better agreement with the data.

E. ^{40}Ca$(d,t)^{39}$Ca Reactions

As mentioned in the Introduction, (d,t) reaction yields were measured at the same time as the $(d,{}^3\mathrm{He})$ data. The ^{40}Ca$(d,t)^{39}$Ca angular distributions obtained are presented in Fig. 21, together with DW predictions using the local zero-range form of the theory. Since no tritium elastic-scattering data is available at the appropriate energies, the same optical-model potential as used above for the ^{3}He scattering has been used. It can be seen from Fig. 21 that this potential results in excellent fits to the observed angular distributions.

TABLE VII. Spectroscopic factors from ^{40}Ca$(d,t)^{39}$Ca.

^{39}Ca level (MeV)	Configuration	C^2S LZR
0	$(1d_{3/2})^{-1}$	4.84
2.42	$(2s_{1/2})^{-1}$	1.83
2.74	$(2s,1d)^{-2}(1f_{7/2})^1$	0.43
5.02	$(1d_{5/2})^{-1}$	1.66

Table VII contains spectroscopic factors resulting from the comparison of experiment and theory for the (d,t) reactions. In these cases we use the same normalization[20] for (d,t) as for $(d,{}^3\mathrm{He})$ reactions, namely

$$\frac{d\sigma}{d\Omega}(d,t)=2.95C^2S\sigma_{\mathrm{DW}}(\theta).$$

A comparison of Tables VI and VII shows agreement to within 20% for the mirror states observed in both $(d,{}^3\mathrm{He})$ and (d,t). This is as good as might be expected, considering the experimental and theoretical uncertainties.

The third excited state was observed at some angles at an energy corresponding to 2.96±0.06 MeV in ^{39}Ca. Similarly, states were observed at 5.37±0.10 MeV and 6.03±0.10 MeV in ^{39}Ca, which are most likely the $1d_{5/2}$ hole states reported at 5.48 and 6.15 MeV.[11,12] Background problems prohibited obtaining angular distributions for these higher excited levels.

VI. DISCUSSION

The primary motivation for the present investigation was to test the reliability of the distorted-wave theory, as currently used, to predict differential cross sections for $(d,{}^3\mathrm{He})$ reactions. The results of this investigation indicate that the theory is capable of predicting both the shape and magnitude of these cross sections. The finite-range form of the theory results in spectroscopic factors which agree with the shell-model predictions for the three reactions studied to within 7%. It is now apparent from this and other investigations that the ^{16}O and ^{40}Ca nuclei do not have completely closed-shell configurations; thus the errors are somewhat larger than 7%. A reliability of ±20% can safely be assigned to the predictions with this version of the theory.

The local zero-range form of the theory also reproduces angular distribution shapes and predicts magnitudes to within 20% of the shell-model expectations. Although the finite-range form is to be preferred, this simplest form of the theory can be used to extract reliable spectroscopic information from experimental data. The nonlocal form consistently underestimates spectroscopic factors due to the larger bound-state wave-function tail. These results suggest that the nonlocality range of 0.85 for the shell-model potential is too large

in these cases. Indeed, it may be more correct to make nonlocality modifications in the distorted waves alone. This prescription was used for the N(0) and K(0) reactions, resulting in spectroscopic factors of 2.20 and 4.68, respectively.

It is encouraging to see the good agreement between DW predictions based on optical-model potentials resulting from actual measurement of the appropriate elastic scattering and those resulting from a systematic study of how the potential parameters vary as a function of target nucleus, i.e., the deuteron "average" potentials of Table I. A similar systematic survey would be useful for the ^{3}He parameters. As discussed in Ref. 3, because of the strong-absorption character of deuteron and ^{3}He scattering, the main features of the predicted differential cross sections for stripping and pickup reactions are not highly sensitive to the precise values of the optical model parameters. These average potentials determined from systematic studies of elastic scattering should prove adequate for the DW analysis of stripping and pickup reactions.

The second part of this investigation points up some of the major difficulties in using the present form of the DW theory. Two problems have been encountered, the first having to do with the proper calculation of the proton wave functions when the proton configurations are mixed, and the second being the failure to include higher order terms in the potential occurring in the DW amplitude (1). The problem of proper binding energy is interesting since the ^{40}Ca$(p,d)^{39}$Ca(2) angular distribution[11] was better reproduced with an effective binding energy, whereas the present ^{40}Ca$(d,^3$He) and ^{40}Ca(d,t) results reported here are better reproduced using separation energies as binding energies. As discussed above, values of C^2S derived with the B_{sep} prescription are to be considered upper limits and further study of this problem is required.

The presence of effects due to the ignored terms in the interaction (2), namely V_{dB} which can produce core excitation, is open to question in the ^{16}O$(d,^3$He) reactions. Further experimental work on the weakly excited levels observed in ^{15}N is in progress to obtain more evidence concerning the presence of core excitation. The ^{12}C$(d,^3$He) study[51] certainly presents evidence for core excitation.

On the basis of our present understanding of the $(d,^3$He) reaction mechanisms, both of the doubly-magic nuclei, ^{16}O and ^{40}Ca, show small departures from pure closed-shell configurations. This conclusion is also evident for the neutron shells based on (p,d) and (d,t) studies quoted above.

Note added in proof. Recent evidence[44] indicates that the 177-MeV potential (potential J in Table II) provides a satisfactory description of ^{3}He scattering from ^{40}Ca in the energy range from 22 to 64 MeV. Using this potential we have repeated the DW calculations for the reactions to the ground and first excited states of ^{39}K using the zero-range, nonlocal, and finite-range forms of the theory. In no case is the shape of the angular distribution significantly altered for $\theta<50°$. However, the spectroscopic factors are reduced from the values shown in Tables III andVI. For the K(0) reaction the three calculations result in a 15–17% reduction; i.e., $C^2S=3.52$ in the finite-range calculation. In the K(1) reaction the reduction varies from 20–35% with the nonlocal calculation having the greatest reduction. In this case $C^2S(\text{FR})=1.29$.

ACKNOWLEDGMENTS

The authors are indebted to R. M. Drisko and G. R. Satchler for helpful comments and discussions, and to J. K. Dickens for his aid in making available the LEA computer program. We also wish to thank the cyclotron crew for their cooperation in performing the experiments.